Gut stem cell necroptosis by genome instability triggers bowel inflammation

https://doi.org/10.1038/s41586-020-2127-x

Received: 17 July 2019

Accepted: 24 January 2020

Ruicong Wang[1,2,7], Hongda Li[1,2,7], Jianfeng Wu[1,2,7], Zhi-Yu Cai[1,2,7], Baizhou Li[3], Hengxiao Ni[1,2], Xingfeng Qiu[4], Hui Chen[5], Wei Liu[1,2], Zhang-Hua Yang[1,2], Min Liu[1,2], Jin Hu[1,2], Yaoji Liang[1], Ping Lan[6], Jiahuai Han[1,2]✉ & Wei Mo[1,2]✉

The aetiology of inflammatory bowel disease (IBD) is a multifactorial interplay between heredity and environment[1,2]. Here we report that deficiency in SETDB1, a histone methyltransferase that mediates the trimethylation of histone H3 at lysine 9, participates in the pathogenesis of IBD. We found that levels of SETDB1 are decreased in patients with IBD, and that mice with reduced SETDB1 in intestinal stem cells developed spontaneous terminal ileitis and colitis. SETDB1 safeguards genome stability[3], and the loss of SETDB1 in intestinal stem cells released repression of endogenous retroviruses (retrovirus-like elements with long repeats that, in humans, comprise approximately 8% of the genome). Excessive viral mimicry generated by motivated endogenous retroviruses triggered Z-DNA-binding protein 1 (ZBP1)-dependent necroptosis, which irreversibly disrupted homeostasis of the epithelial barrier and promoted bowel inflammation. Genome instability, reactive endogenous retroviruses, upregulation of ZBP1 and necroptosis were all seen in patients with IBD. Pharmaceutical inhibition of RIP3 showed a curative effect in SETDB1-deficient mice, which suggests that targeting necroptosis of intestinal stem cells may represent an approach for the treatment of severe IBD.

To find critical molecules that cause or favour the development of IBD, we analysed whole-genome transcriptome profiling data from patients with IBD[4], which showed that SETDB1 was nearly cut in half in samples from patients compared to tissues from unaffected controls (Fig. 1a). The reduction of SETDB1 protein was confirmed in biopsy specimens (including inflamed regions) from patients with IBD (Fig. 1b). SETDB1 expression was restricted in epithelial stem cells in normal crypts (Fig. 1c, orange arrowhead) and decreased in patients with IBD (Fig. 1d, Extended Data Fig. 1a). SETDB1 was deleted in the mouse intestinal epithelium by generating VIL–CreERT2 *Setdb1*$^{fl/fl}$ mice, which show tamoxifen-inducible knockout of *Setdb1* in intestinal epithelial cells (IECs); *Setdb1*$^{iIEC\text{-}KO}$ refers to tamoxifen-induced VIL–CreERT2 *Setdb1*$^{fl/fl}$ mice. Considering the fact that environmental factors become influential postnatally and that the onset of IBD happens frequently in young adults[5], adult mice were treated with tamoxifen (Extended Data Fig. 1b) to completely delete *Setdb1* in intestinal epithelium as detected by immunohistochemical (IHC) staining at three days post-induction (dpi) (Extended Data Fig. 1c). *Setdb1*$^{iIEC\text{-}KO}$ mice had severe enteritis with reduced body weight (Extended Data Fig. 1d) and diarrhoea at 5 dpi. Endoscopic examination showed mucosal thickening, ulceration and ischaemic lesions (Fig. 1e) in the *Setdb1*-knockout colon. The mutant mice had intestinal oedema (Extended Data Fig. 1e) and most of them died at around 10 dpi (Extended Data Fig. 1f). Pathological anatomy confirmed the diagnosis of terminal ileitis and colitis in *Setdb1*$^{iIEC\text{-}KO}$ mice at 8 dpi. The terminal ileum exhibited destroyed epithelium with atrophy of the villi and crypt deformation (Fig. 1f). More Ki67$^+$ proliferative cells, and fewer MUC2$^+$ goblet cells and disordered lysozyme$^+$ Paneth cells, were observed (Extended Data Fig. 2a, b). The colon showed deformity at 8 dpi (Fig. 1f) and severe barrier breakdown at 10 dpi (Extended Data Fig. 2c). The epithelial barriers of VIL–CreERT2 mice remained intact (Extended Data Fig. 2d). There were expanding infiltrated lymphocytes in the lamina propria and epithelium of *Setdb1*$^{iIEC\text{-}KO}$ mice, indicating that a strong bowel inflammation is caused by *Setdb1* deletion (Fig. 1g).

Consistent with pathological diagnosis, the transcriptome landscape of guts in which *Setdb1* was deleted presented a bowel inflammatory signature (Fig. 1h). Substantial reductions of mucins and antimicrobial peptides (Fig. 1i), upregulated TNF and other pro-inflammatory cytokines, as well as chemokines, were observed in *Setdb1*-knockout intestines (Extended Data Fig. 2e). A similar inflammatory pathology was also observed in VIL–Cre *Setdb1*$^{fl/fl}$ mice, most of which died within the first two weeks of life (Extended Data Fig. 3a). A few of these mice that showed uneven knockout efficiency lived up to 3–7 weeks (Extended Data Fig. 3b) and developed adenoma in 100% penetration (Extended Data Fig. 3c), which is consistent with clinical observations of a higher risk of developing tumours in patients with IBD[6]. All mutant mice had abnormal bowel architecture with inflammation (Extended Data Fig. 3d–f). Given the higher SETDB1 expression in intestinal stem cells (ISCs) and the fact that a similar bowel inflammatory pathology

---

[1] State Key Laboratory of Cellular Stress Biology, Innovation Center for Cell Signaling Network, School of Life Sciences, Xiamen University, Xiamen, China. [2] Cancer Research Center, Xiang'an Hospital, School of Medicine, Xiamen University, Xiamen, China. [3] Department of Pathology, The Second Affiliated Hospital of Zhejiang University School of Medicine, Hangzhou, China. [4] Department of Gastrointestinal Surgery, Zhong Shan Hospital, Xiamen University, Xiamen, China. [5] Department of Gastroenterology, The First Affiliated Hospital of Fujian Medical University, Fuzhou, China. [6] Department of Gastroenterology, The Sixth Affiliated Hospital, Sun Yat-sen University, Guangzhou, China. [7] These authors contributed equally: Ruicong Wang, Hongda Li, Jianfeng Wu, Zhi-Yu Cai. ✉e-mail: jhan@xmu.edu.cn; wmo@xmu.edu.cn

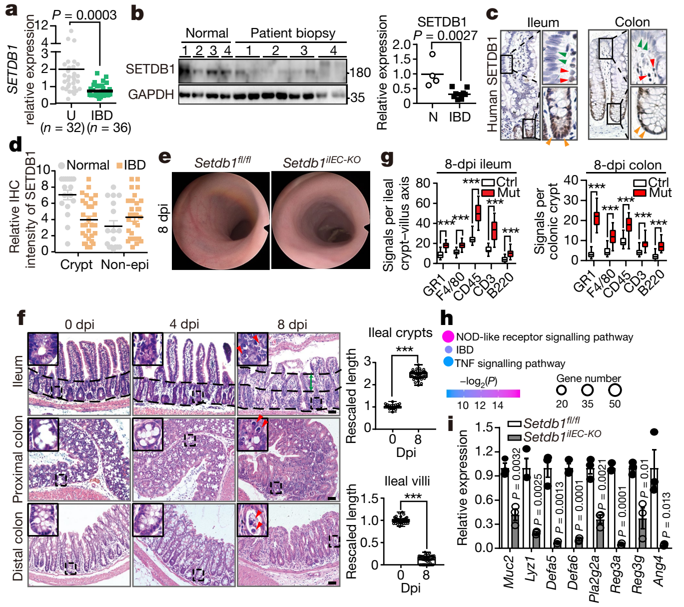

Fig. 1 | Epithelial SETDB1 depression triggers IBD. a, *SETDB1* expression in patients with IBD (IBD) ($n = 36$) and unaffected controls (U) ($n = 32$), revealed by analysing a database of RNA-sequencing data (Gene Expression Omnibus (GEO) accession number GSE112366). **b**, SETDB1 protein in normal intestinal tissues (N) ($n = 4$) and biopsies from patients with IBD ($n = 4$), with quantifications shown on the right. The two lanes with the same patient number are two biopsies that were collected under the endoscope at the same time. **c**, SETDB1 IHC in normal human ileum and colon. Boxed regions are shown in high magnification on the right. Orange, green and red arrowheads show crypts, villi and non-epithelial cells, respectively. $n = 3$ individual experiments were repeated. **d**, SETDB1 IHC intensity in normal tissue ($n = 17$) and surgical specimens from patients with IBD ($n = 30$). Data shown here are related to those in Extended Data Fig. 1a. Details of statistical quantification are provided in Methods. Non-epi, non-epithelial cells. **e**, Endoscopic images of the colon at 8 dpi ($n = 3$ mice). **f**, Haematoxylin and eosin (H & E) staining of intestinal sections. Five or more mice were stained for each time point, with similar results. Green arrows between the two dashed lines show elongated crypts. Insets show crypt bottom with detached cells. Graphs on the right are lengths of ileal crypts and villi (50 crypt–villus axes were counted). Details of statistical quantification are provided in Methods. **g**, Lymphocyte IHC signals in ileum or colon of *Setdb1*$^{fl/fl}$ (Ctrl) and *Setdb1*$^{iIEC\text{-}KO}$ (Mut). $n = 50$ crypt–villus axes; statistics are the same as in Figs. 3f, 4e and Extended Data Fig. 3f. Three individual experiments were repeated. Data shown here are related to those in Supplementary Fig. 3. **h**, Bowel inflammatory signature of ileal crypts in 4-dpi *Setdb1*$^{iIEC\text{-}KO}$ mice ($n = 1$ mouse). *P* value determination is described in Methods. The size of the circles in the bottom right represents the number of differentially expressed genes. **i**, Quantitative (q)PCR of antimicrobial peptides and mucins of intestinal crypts at 4 dpi ($n = 3$ mice). Scale bars, 50 μm. Data are mean ± s.e.m. Box plots show median and 25th to 75th percentiles, and whiskers indicate the minimum and maximum values. *P* values are determined by two-sided, unpaired *t*-test. ***$P \leq 0.001$.

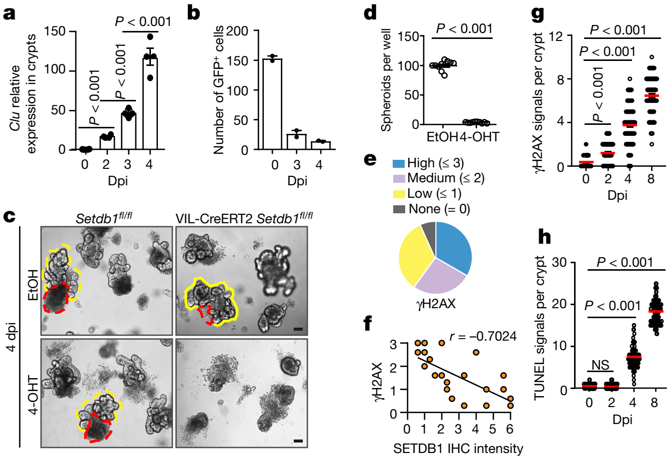

Fig. 2 | Bowel inflammation is associated with genome instability and stem cell death. a, qPCR of *Clu* expression level from mouse crypts at continuous dpi ($n = 4$ mice for each day). **b**, Numbers of GFP$^+$ cells from a continuous 50 crypts of *Lgr5-eGFP-Setdb1*$^{iIEC\text{-}KO}$ mice after tamoxifen induction. $n = 2$ mice for each day. **c**, Representative images of 4-dpi organoids grown in ENR medium ($n = 6$ experimental repeats).Yellow lines, live organoids; red lines, cells undergoing anoikis. **d**, Numbers of single ISC-derived spheroids per well ($n = 10$ wells) from VIL–CreERT2 *Setdb1*$^{fl/fl}$ mice treated with 4-hydroxytamoxifen (4-OHT), or EtOH as control. Data shown are related to those in Extended Data Fig. 4g. **e**, Plot of γH2AX IHC. $n = 30$ surgical samples from patients with IBD. Details of the analysis strategy are included in Methods. **f**, Correlation analysis for γH2AX and SETDB1 in patients ($n = 23$). Details of the determination of correlation are shown in Methods. **g**, **h**, Numbers of γH2AX$^+$ and TUNEL$^+$ cells in crypts. Data shown are related to those in Extended Data Fig. 4i. A total of 100 intact crypts (from 3 experimental repeats) were counted each day. Scale bars, 50 μm. Data are mean ± s.e.m. *P* values were determined by two-sided unpaired *t*-test. NS, not significant.

was seen in mice with ISC-specific *Setdb1* deletion (by *Olfm4-creERT2*) (Extended Data Fig. 3g), we concluded that deletion of *Setdb1* in ISCs triggers bowel inflammation in mice.

Whole-genome transcriptome sequencing using crypts at continuous time points after tamoxifen administration (Extended Data Fig. 4a) revealed the activation of innate immunity from 2 dpi (Extended Data Fig. 4b). Differentially expressed genes at 2, 3 and 4 dpi are shown as volcano plots (Extended Data Fig. 4c). *Clu*, a unique marker of revival stem cells for intestinal regeneration upon damage to ISCs[7] (Extended Data Fig. 4d), emerged at the top of the list of the most significantly (statistics provided in Methods, Extended Data Table 1) upregulated genes (Fig. 2a, Extended Data Table 1), suggesting stem cell death in *Setdb1*-knockout crypts. This was further verified by the disappearance of majority of GFP signals in *Lgr5-eGFP-Setdb1*$^{iIEC\text{-}KO}$ mice at 3 dpi (Fig. 2b, Extended Data Fig. 4e). Intrinsic ISC death was reproduced ex vivo in medium containing EGF, Noggin and R-spondin (ENR medium) for 3D mini-gut organoid culture. Organoids with *Setdb1* deletion stopped fission and did not generate a crypt–villus structure (Fig. 2c). Propidium iodide staining revealed abundant cell death (Extended Data Fig. 4f). Spheroids consisting of ISCs showed disintegration upon *Setdb1* ablation, which illustrated the death of stem cells (Fig. 2d, Extended Data Fig. 4g). As SETDB1 maintains chromosomal stability[8], we propose that the genome instability caused by SETDB1 inactivation leads to ISC death. Twenty-two of thirty surgical specimens showed signals of staining for γH2AX (Fig. 2e), a marker of DNA double-strand break foci used to assess genome instability. A strong correlation between SETDB1 depression and genome instability was established by analysing the IHC staining intensity of SETDB1 and γH2AX (Fig. 2f, Extended Data Fig. 4h). The appearance of γH2AX in *Setdb1*$^{iIEC\text{-}KO}$ crypts (Fig. 2g, Extended Data Fig. 4i) was synchronous with acute expression of *Clu* (Fig. 2a), implying a tight bond between genome instability and death of ISCs. Obvious ISC death was detected at 4 dpi by the TdT-mediated dUTP nick-end labelling (TUNEL) assay (Fig. 2h, Extended Data Fig. 4i), which detects apoptosis and other types of cell death[9,10]. Thus, bowel inflammation in *Setdb1*$^{iIEC\text{-}KO}$ mice is associated the death of ISCs caused by genome instability.

Genome instability could potentiate inflammation and trigger apoptosis[11–13]. However, blocking apoptosis in *Setdb1*$^{iIEC\text{-}KO}$ mice by introducing a further knockout of *Casp8* in IECs did not attenuate epithelial damage, but instead aggravated it (Extended Data Fig. 5a); ex vivo caspase inhibition with zVAD-fmk, a pan-caspase inhibitor, did not rescue cell death in *Setdb1*-null organoids (Extended Data Fig. 5b).

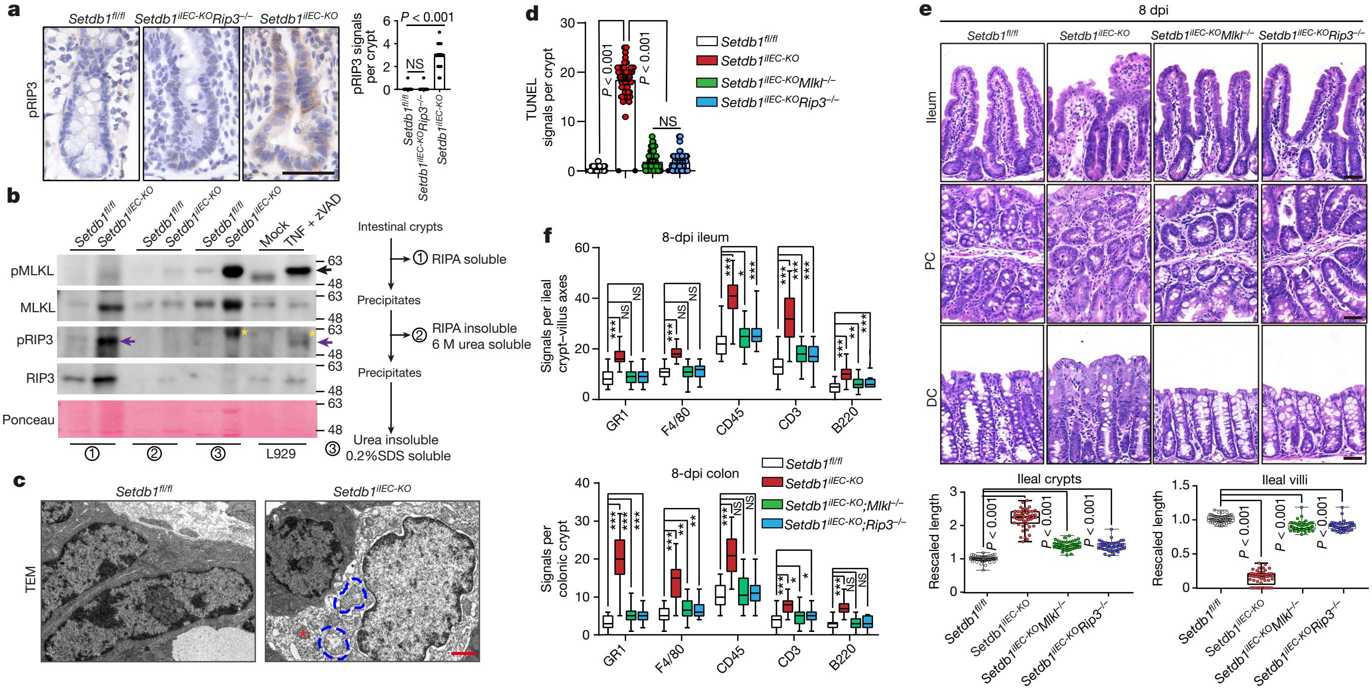

Fig. 3 | Necroptosis in SETDB1-deficient crypts links cell death to inflammation. a, IHC of phosphorylated (p)RIP3 in ileal crypts at 6 dpi, as indicated. Ileal crypts from *Setdb1*$^{iIEC\text{-}KO}$ *Rip3*$^{-/-}$ mice at 6 dpi were included as negative control for pRIP3 IHC. The graph on the right is the quantification of pRIP3. $n = 20$ crypts. **b**, Proteins are extracted from intestinal crypts at 8 dpi, following the schematic procedure. Cell lysates of L929 cells treated with TNF and zVAD-fmk (zVAD) were used as a positive control for both pMLKL and pRIP3. For pRIP3, arrows point to specific bands and asterisks denote non-specific bands. The specificities of pMLKL and pRIP3 antibodies are further confirmed in Supplementary Fig. 4b. **c**, Electron microscopy images of necrotic-like ileal crypt cells in 4-dpi *Setdb1*$^{iIEC\text{-}KO}$ mice. Dotted blue lines encircled the swelling mitochondrion. Asterisk marks the low electronic condensation of cytoplasm. $n = 2$ mice. TEM, transmission electron microscopy. **d**, Numbers of TUNEL$^+$ cells in ileal crypts. Data shown here are related to those in Extended Data Fig. 5d. Fifty intact ileal crypts were checked. The same experiment was performed four times. **e**, H & E staining of ileum, proximal colon (PC) and distal colon (DC) at 8 dpi from mice of different genotypes (as indicated). $n = 3$ mice. Bottom, lengths of ileal crypts and villi as indicated ($n = 50$ crypts or villi). **f**, Lymphocyte IHC signals in ileum or colon. $n = 50$ crypt–villus axes. Details are shown in Supplementary Fig. 3. Scale bars, 50 μm (**a**, **e**), 1 μm (**c**). Data are mean ± s.e.m. Box plots show median and 25th to 75th percentiles, and whiskers indicate the minimum and maximum values. *P* values are determined by two-sided unpaired *t*-test. NS, not significant; $^*P \leq 0.05$; $^{**}P \leq 0.01$; $^{***}P \leq 0.001$.

Necroptosis, a type of cell death that is independent of caspase, has previously been observed in a mouse model of enteritis when either *Casp8* or *Fadd* was ablated in IECs[9,14]. Although the genome instability caused by SETDB1 inactivation has not previously been documented as causing necroptosis, phosphorylated RIP3 and phosphorylated MLKL—the hallmarks of necroptosis—were detected in *Setdb1*-knockout crypts by IHC and western blot (Fig. 3a, b, Extended Data Fig. 5c). Transmission electron microscopy images also showed subcellular features of necrosis-like swelling mitochondria and a low electronic condensation of cytoplasm (Fig. 3c). To evaluate the pathological contribution of necroptosis, we used the deletion of *Mlkl* or *Rip3* (also known as *Ripk3*) to block necroptosis in vivo. Compared with *Setdb1*-mutant crypts, the number of dying cells was greatly reduced in crypts of *Setdb1*-knockout *Mlkl*$^{-/-}$ or *Setdb1*-knockout *Rip3*$^{-/-}$ mice (Fig. 3d, Extended Data Fig. 5d). Consequentially, the integrity of intestinal epithelium was restored (Fig. 3e) and the invasion of immune cells was largely inhibited (Fig. 3f), indicating that necroptosis by genome instability links stem cell death to bowel inflammation.

Necroptosis induced by the proinflammatory cytokine TNF is a prototypical model of necroptosis, for which RIP1 is required[15]. Although there was a high level of TNF in organoids with SETDB1 inactivation (Extended Data Fig. 6a), neither TNF neutralization by TNF antibody nor RIP1 kinase inhibition by the RIP1 inhibitor Nec-1 impeded the deterioration of organoids (Extended Data Fig. 6b). The RIP3 inhibitor GSK'872 rescued *Setdb1*-deficient organoids from cell death (Extended Data Fig. 6b), indicating genomic instability leads to necroptosis in a RIP1-independent manner.

ZBP1 interacts with RIP3 via its receptor-interacting protein homotypic interaction motif (RHIM) domain to trigger necroptosis[10,16]. The recruitment of RIP3 by ZBP1 was detectable from 4 dpi in *Setdb1*$^{iIEC\text{-}KO}$ crypts (Fig. 4a). Genetic ablation of *Zbp1* abrogated RIP3 activation (Fig. 4b, Extended Data Fig. 7a) and eliminated cell death almost completely in vivo (Fig. 4c, Extended Data Fig. 7b). Sequentially, the villus atrophy (Fig. 4d) and lymphocyte infiltration (Fig. 4e) were largely attenuated in *Setdb1*$^{iIEC\text{-}KO}$ *Zbp1*$^{-/-}$ double-knockout mice, indicating ZBP1 is a key mediator of RIP3 activation for necroptosis by *Setdb1* deletion. Increased levels of ZBP1 and phosphorylated MLKL were observed in patients with IBD, indicating that there is a correlation between ZBP1 and necroptosis in these patients (Fig. 4f); however, we cannot exclude the possibility that the increase of ZBP1 is a consequence rather than a cause of the disease.

We used KEGG (Kyoto Encyclopedia of Genes and Genomes) analysis to comprehensively describe the intracellular environment required to activate ZBP1 for necroptosis in *Setdb1*-knockout crypts, which revealed a coupled activation of multiple viral infections and antiviral host-defence pathways (Fig. 4g). It is known that silencing SETDB1 in acute myeloid leukaemia leads to the expression of type I interferon[3]. The level of IFNβ in *Setdb1*-null organoids was about sixfold that in wild-type organoids (Extended Data Fig. 7c, left). *Zbp1* is an interferon-stimulated gene that is upregulated in *Setdb1*-knockout crypts and organoids (Extended Data Fig. 7c right, d). Other interferon-stimulated genes were also upregulated (Extended Data Fig. 7e). The ZBP1 induced by IFNβ in *Setdb1* wild-type organoids (about 4-fold at 4 dpi) (Extended Data Fig. 7f) cannot promote cell death in wild-type organoids

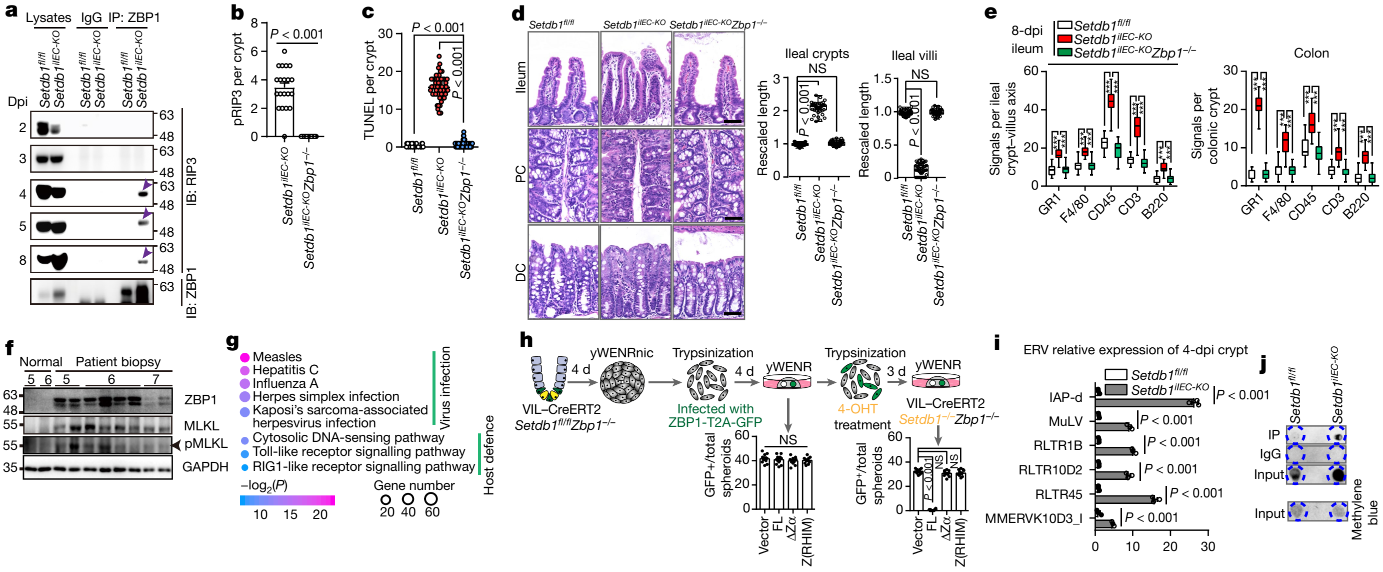

Fig. 4 | ZBP1 senses ERV RNA and recruits RIP3 for necroptosis upon genome instability by SETDB1 deficiency. a, RIP3 in the immunoprecipitates of ZBP1 from a series of intestinal crypts from tamoxifen-induced mice. *n* = 3 mice. The specificity of ZBP1 antibody for immunoprecipitation is validated in Supplementary Fig. 5. IB, immunoblot. **b**, Numbers of pRIP3 cells per crypt identified by IHC. *n* = 20 crypts. Data shown are related to those in Extended Data Fig. 7a. **c**, Numbers of TUNEL$^+$ cells per crypt. Fifty intact crypts were examined. Data shown are related to those in Extended Data Fig. 7b. **d**, H & E staining of ileum and colon. Plots to the right show crypt and villi length (*n* = 50 crypts or villi). **e**, Lymphocyte IHC signals in ileum or colon. *n* = 50 crypt–villus axes. **f**, ZBP1, MLKL and pMLKL expression in biopsies from patients; repeated three times with similar results. **g**, Global transcriptome of 4-dpi ileal crypts shows multiple viral infection and host defence responses of upregulated differentially expressed genes. *n* = 1 mouse. *P* value determination is described in Methods. **h**, ZBP1–T2A–GFP, ZBP1(ΔZα) (ΔZα) or ZBP1(RHIM) (Z(RHIM)) mutants were expressed in ISCs (VIL–CreERT2 *Setdb1*$^{fl/fl}$ *Zbp1*$^{-/-}$ mice) (Extended Data Fig. 7h). The percentage of GFP$^+$ spheroids is shown in the left histogram. After *Setdb1* deletion by treatment with 4-OHT, the percentage of GFP$^+$ spheroids (Extended Data Fig. 7i) is shown in the right histogram (*n* = 10 wells). This experiment was repeated three times. FL, full-length ZBP1; yWENR, ENR medium supplemented with WNT3A and Y-27632. **i**, qPCR verification of relative expression of ERVs from 4-dpi intestinal crypts. *n* = 3 experimental repeats. The *y*-axis labels refer to mouse ERVs, details of which can be found in ref. [19]. IAP, intracisternal A particle; MulV, murine leukaemia virus. **j**, Cross-link immunoprecipitation assay shows the binding of ZBP1 with dsRNA. Further details are provided in Extended Data Fig. 7n. *n* = 3 experimental repeats. Scale bars, 50 μm. Data are mean ± s.e.m. Box plots show median and 25th to 75th percentiles, and whiskers indicate the minimum and maximum values. *P* values were determined by two-sided unpaired *t*-test. ***$P \leq 0.001$.

(Extended Data Fig. 7g); whereas the approximately twofold ZBP1 upregulation in *Setdb1*-null organoids evidently induced cell death (Extended Data Fig. 7g). Blocking IFNβ with anti-IFNAR neutralizing antibody eliminated IFNβ-induced ZBP1 expression in wild-type organoids (Extended Data Fig. 7f), but did not inhibit ZBP1 upregulation (Extended Data Fig. 7g) or cell death in *Setdb1*-null organoids (Extended Data Fig. 7g). This suggests that the induction of cell death in organoids requires not only the upregulation of ZBP1 but also an unknown factor or factors to initiate ZBP1-mediated necroptosis. IFNβ is not required for cell death in *Setdb1*-null organoids ex vivo in our experimental setting, but its participation in the pathological changes that are mediated by *Setdb1* in vivo cannot be excluded.

ZBP1 has two nucleic-acid binding domains, Zα1and Zα2. Zα2 has previously been reported to sense genomic RNA of the influenza A virus for cell death[17,18]. Therefore, we examined whether the Zα domains were required for ZBP1-mediated necroptosis in *Setdb1*$^{-/-}$ ISCs. VIL–CreERT2 *Setdb1*$^{fl/fl}$ *Zbp1*$^{-/-}$ ISCs were reconstituted with full-length ZBP1, ZBP1 with the Zα1 and Zα2 domains deleted (ZBP1(ΔZα)) or ZBP1 with a mutant RHIM domain (ZBP1(RHIM)) (Extended Data Fig. 7h). Lentiviral infection yielded about 40% GFP$^+$ spheroids in each group. Reconstituting the expression of ZBP1 and its mutants had no effect on the survival of *Setdb1* wild-type, *Zbp1*$^{-/-}$ ISCs, as shown by the fact that the ratio of GFP$^+$ spheroids was comparable in all groups at four days after infection (Fig. 4h, left histogram). After *Setdb1* was deleted, *Setdb1*$^{-/-}$ *Zbp1*$^{-/-}$ ISCs reconstituted with vector, ZBP1(RHIM) and ZBP1(ΔZα) maintained the original proportions of GFP$^+$ spheroids whereas GFP$^+$ spheroids were barely found in *Setdb1*$^{-/-}$ *Zbp1*$^{-/-}$ ISCs reconstituted with full-length ZBP1 (Fig. 4h, right histogram, Extended Data Fig. 7i). The requirement of both of the Zα domains and the RHIM domain suggested that ZBP1 senses 'viral' RNA through its Zα domains and recruits RIP3 through its RHIM domain in necroptosis caused by *Setdb1* deletion.

Considering there was no viral infection in *Setdb1*-knockout ISCs, de-repressed endogenous RNA in cells could function as viral RNA to prime ZBP1 for necroptosis. Massive double-stranded (ds)RNAs were detected in *Setdb1*-knockout crypts and organoids (Extended Data Fig. 7j, k). RNA sequencing for repeats revealed that large endogenous retroviruses (ERVs) were dysregulated in *Setdb1*-knockout crypts, presenting a unique profile compared with the activation of ERVs in other tissues (Extended Data Fig. 7l). Because the SETDB1-mediated trimethylation of histone H3 at Lys9 (H3K9me3) maintains genome integrity by enforcing the repression of ERVs[19], we performed H3K9me3 chromatin immunoprecipitation with sequencing, which revealed that 25 reactive ERVs were regulated by H3K9me3 *in cis* (Fig. 4i, Extended Data Fig. 7m). A cross-link immunoprecipitation assay[20] (Extended Data Fig. 7n) in *Setdb1*-knockout crypts showed the binding of ZBP1 with dsRNAs (Fig. 4j), which we found to be ERV RNAs by sequencing the PCR products from ZBP1 immunoprecipitates (Extended Data Fig. 7o). Collectively, our data strongly suggested that RNAs from reactivated ERVs bind and activate ZBP1 for necroptosis mediated by *Setdb1* deletion in ISCs. Despite the high sequential variability of ERVs between species, we also observed the dysregulation of viral mimicry in patients with IBD through an analysis of a public database of repeat sequencing[21] (Extended Data Fig. 7p).

Because SETDB1 in patients with IBD is reduced rather than abolished, we examined *Setdb1*-heterozygous (VIL–CreERT2 *Setdb1*$^{fl/+}$; hereafter, *Setdb1*$^{iIEC-Het}$—referring to induced VIL–CreERT2 *Setdb1*$^{fl/+}$mice) mice

(Extended Data Fig. 8a). The *Setdb1*$^{iIEC\text{-}Het}$ mice showed mild symptoms of bowel inflammation (Extended Data Fig. 8b–f) after tamoxifen induction. A few of the *Setdb1*$^{iIEC\text{-}Het}$ mice developed destroyed epithelium (Extended Data Fig. 8g). Semi-deletion of *Setdb1* generated more dead cells ex vivo than did *Setdb1*$^{fl/fl}$ in organoid culture (Extended Data Fig. 8h). In addition, mice with mosaic *Setdb1* deletion in intestinal epithelium by VIL–Cre also showed bowel inflammatory pathology (Extended Data Fig. 3c–f).

The luminal microbiota could be involved in the pathogenesis of IBD under particular circumstances[1]. However, when the intestinal microbiota was eliminated, the epithelial architecture of *Setdb1*$^{iIEC\text{-}KO}$ mice showed little amelioration at 8 dpi (Extended Data Fig. 9a), which excludes a vital role for the microbiota in bowel inflammation by SETDB1 deficiency. Genetic deletion of *Mlkl* or *Rip3* obviously prolonged (whereas deletion of *Casp8* even shortened) the lifespan of *Setdb1*$^{iIEC\text{-}KO}$ mice (Extended Data Fig. 9b). Administration of a high dose of GSK'872 showed partially curative effects in these mice (Extended Data Fig. 9b, c). *Setdb1*$^{iIEC\text{-}KO}$ *Rip3*$^{-/-}$ mice had slightly longer survival time than that of *Setdb1*$^{iIEC\text{-}KO}$ *Mlkl*$^{-/-}$ mice, probably because RIP3 has an additional role in cytokine production[22]. Neither *Rip3* nor *Mlkl* deletion had as marked an effect as that of *Zbp1* knockout in rescuing the death of *Setdb1*$^{iIEC\text{-}KO}$ mice. *Setdb1*$^{iIEC\text{-}KO}$ *Zbp1*$^{-/-}$ mice looked healthy and none of them died during the entire period under observation. Necroptosis could switch to apoptosis when *Rip3* or *Mlkl* is deleted[23–25]; this is likely to be the case here, as shown by the fact that an additional deletion of *Casp8* in the *Setdb1*$^{iIEC\text{-}KO}$ *Rip3*$^{-/-}$ background extended the lifespan of the mice to a period comparable to that of the *Setdb1*$^{iIEC\text{-}KO}$ *Zbp1*$^{-/-}$ mice (Extended Data Fig. 9b). ZBP1 could trigger the parallel pathways of apoptosis and necroptosis[20,21] but it seems that the role of apoptosis in contributing to the pathology of *Setdb1*$^{iIEC\text{-}KO}$ mice is not critical, because *Casp8* deletion or inhibition did not attenuate—but instead even enhanced—the epithelial damage induced by *Setdb1* deficiency (Extended Data Fig. 5a, b). Collectively, necroptosis is the primary cause of death for *Setdb1*$^{iIEC\text{-}KO}$ mice. Genome instability caused by *Setdb1* deficiency in ISCs induces ZBP1-mediated necroptosis, which triggers bowel inflammation (Extended Data Fig. 10). Interfering with the sensing of ERV RNA by ZBP1 may provide benefits in the treatment of auto-inflammation in patients with IBD.

Online content

Any methods, additional references, Nature Research reporting summaries, source data, extended data, supplementary information, acknowledgements, peer review information; details of author contributions and competing interests; and statements of data and code availability are available at https://doi.org/10.1038/s41586-020-2127-x.

1. de Souza, H. S. P., Fiocchi, C. & Iliopoulos, D. The IBD interactome: an integrated view of aetiology, pathogenesis and therapy. *Nat. Rev. Gastroenterol. Hepatol*. **14**, 739–749 (2017).
2. Ananthakrishnan, A. N. et al. Environmental triggers in IBD: a review of progress and evidence. *Nat. Rev. Gastroenterol. Hepatol*. **15**, 39–49 (2018).
3. Cuellar, T. L. et al. Silencing of retrotransposons by SETDB1 inhibits the interferon response in acute myeloid leukemia. *J. Cell Biol*. **216**, 3535–3549 (2017).
4. VanDussen, K. L. et al. Abnormal small intestinal epithelial microvilli in patients with Crohn' s disease. *Gastroenterology* **155**, 815–828 (2018).
5. Peloquin, J. M., Goel, G., Villablanca, E. J. & Xavier, R. J. Mechanisms of pediatric inflammatory bowel disease. *Annu. Rev. Immunol*. **34**, 31–64 (2016).
6. Choi, C. R., Bakir, I. A., Hart, A. L. & Graham, T. A. Clonal evolution of colorectal cancer in IBD. *Nat. Rev. Gastroenterol. Hepatol*. **14**, 218–229 (2017).
7. Ayyaz, A. et al. Single-cell transcriptomes of the regenerating intestine reveal a revival stem cell. *Nature* **569**, 121–125 (2019).
8. Dodge, J. E., Kang, Y.-K., Beppu, H., Lei, H. & Li, E. Histone H3-K9 methyltransferase ESET is essential for early development. *Mol. Cell. Biol*. **24**, 2478–2486 (2004).
9. Günther, C. et al. Caspase-8 regulates TNF-α-induced epithelial necroptosis and terminal ileitis. *Nature* **477**, 335–339 (2011).
10. Lin, J. et al. RIPK1 counteracts ZBP1-mediated necroptosis to inhibit inflammation. *Nature* **540**, 124–128 (2016).
11. McNairn, A. J., Chuang, C. H., Bloom, J. C., Wallace, M. D. & Schimenti, J. C. Female-biased embryonic death from inflammation induced by genomic instability. *Nature* **567**, 105–108 (2019).
12. Zhang, Y. et al. Heterochromatin anomalies and double-stranded RNA accumulation underlie *C9orf72* poly(PR) toxicity. *Science* **363**, eaav2606 (2019).
13. Chiappinelli, K. B. et al. Inhibiting DNA methylation causes an interferon response in cancer via dsRNA including endogenous retroviruses. *Cell* **162**, 974–986 (2015).
14. Welz, P. S. et al. FADD prevents RIP3-mediated epithelial cell necrosis and chronic intestinal inflammation. *Nature* **477**, 330–334 (2011).
15. Pasparakis, M. & Vandenabeele, P. Necroptosis and its role in inflammation. *Nature* **517**, 311–320 (2015).
16. Newton, K. et al. RIPK1 inhibits ZBP1-driven necroptosis during development. *Nature* **540**, 129–133 (2016).
17. Thapa, R. J. et al. DAI senses influenza A virus genomic RNA and activates RIPK3-dependent cell death. *Cell Host Microbe* **20**, 674–681 (2016).
18. Kuriakose, T. et al. ZBP1/DAI is an innate sensor of influenza virus triggering the NLRP3 inflammasome and programmed cell death pathways. *Sci. Immunol*. **1**, aag2045 (2016).
19. Kato, M., Takemoto, K. & Shinkai, Y. A somatic role for the histone methyltransferase Setdb1 in endogenous retrovirus silencing. *Nat. Commun*. **9**, 1683 (2018).
20. Maelfait, J. et al. Sensing of viral and endogenous RNA by ZBP1/DAI induces necroptosis. *EMBO J*. **36**, 2529–2543 (2017).
21. Wang, W. et al. Metagenomic analysis of microbiome in colon tissue from subjects with inflammatory bowel diseases reveals interplay of viruses and bacteria. *Inflamm. Bowel Dis*. **21**, 1419–1427 (2015).
22. Alvarez-Diaz, S. et al. The pseudokinase MLKL and the kinase RIPK3 have distinct roles in autoimmune disease caused by loss of death-receptor-induced apoptosis. *Immunity* **45**, 513–526 (2016).
23. Han, J., Zhong, C. Q. & Zhang, D. W. Programmed necrosis: backup to and competitor with apoptosis in the immune system. *Nat. Immunol*. **12**, 1143–1149 (2011).
24. Zhang, D. W. et al. RIP3, an energy metabolism regulator that switches TNF-induced cell death from apoptosis to necrosis. *Science* **325**, 332–336 (2009).
25. Remijsen, Q. et al. Depletion of RIPK3 or MLKL blocks TNF-driven necroptosis and switches towards a delayed RIPK1 kinase-dependent apoptosis. *Cell Death Dis*. **5**, e1004 (2014).

Methods

No statistical methods were used to predetermine sample size. The experiments were not randomized and investigators were not blinded to allocation during experiments and outcome assessment.

Mice

Information about the individual mice strains has been included in Supplementary Table 1. VIL–CreERT2 or VIL–Cre mice were crossed with *Setdb1*$^{fl/fl}$ mice to ablate *Setdb1* in IECs or ISCs. VIL–CreERT2 *Setdb1*$^{fl/fl}$ mice were crossed with *Casp8*$^{fl/fl}$, *Mlkl*$^{-/-}$, *Rip3*$^{-/-}$ or *Zbp1*$^{-/-}$ mice to generate inducible double-knockout mice. For induction of VIL–CreERT2- or *Olfm4-creERT2*-mediated recombination, eight-week old mice were received one dose of tamoxifen 400 mg per kg body weight (mg/kg) by gavage. For induction of *Lgr5-eGFP-IRES-creERT2*-mediated recombination, mice were received 1 dose of tamoxifen 200 mg/kg by gavage for 3 consecutive days. Sample sizes for mouse experiments were empirically determined, and mice were randomly assigned to the control or experimental groups. For all experiments, littermates were used as control indicated in each figure. No blinding was necessary for the mouse experiments present here. Sex preference did not existed in the mouse model of bowel inflammation used here. All mice were in the C57BL/6 background and housed in a conventional environment under a 12-h light:dark cycle at the Xiamen University Laboratory Animal Center. All mouse experiments were approved by the Institutional Animal Care and Use Committee and were in strict accordance with good animal practice as defined by the Xiamen University Laboratory Animal Center.

Antibodies and reagents

Information about primary and secondary antibodies has been included in Supplementary Table 1. For intestinal organoid cultures, advanced DMEM/F12 (8118302, GIBCO), N2 (17502-048, GIBCO), B27 (1799273, GIBCO), EGF (10605-HNAE, Sino Biological), Matrigel matrix (356231, Coring) and WNT3A (Peprotech) were purchased; R-spondin 1- and Noggin-expressing HEK293T cells were a gift from L. Hui[26]. For RIP1, RIP3 or caspase blockade experiments, Nec-1 (4311-88-0), GSK'872 (1346546-69-7), zVAD-fmk (187389-52-2) were purchased from MedChemExpress. In vitro monoclonal antibody anti-TNF neutralization antibody and IFNAR blocking antibody were from BioXCell. For induction of Cre recombinase in vivo and in vitro, tamoxifen and 4-OHT were purchased from StruChem and Tocris Bioscience, respectively.

Human tissue specimens

For western blot, the specimens from patients with IBD were collected under endoscopy for periodic review from the First Affiliated Hospital of Fujian Medical University. Paraffin-embedded specimens from patients with IBD were obtained surgically, and were from the Second Affiliated Hospital of Zhejiang University School of Medicine. Control samples were normal tissues of surgical patients, from the Second Affiliated Hospital of Zhejiang University School of Medicine or the Zhong Shan Hospital of Xiamen. Collection of all samples was approved by the local ethical committee and the institutional review board of their respective hospitals. Each patient gave written informed consent and patient data has been made anonymous. Detailed information of patients is included in Supplementary Table 1.

Histology

Mice were anaesthetized before being killed. Small-intestinal tissues were flushed with ice-cold PBS, coiled into a 'Swiss roll' and fixed in 4% PFA for 2 h at 4 °C. For TUNEL staining, TUNEL kit (MK1023, Boster) was used according to the manufacturer instructions. IHC staining or immunofluorescence was performed as previously described[27]. Microscopy images were captured by Zeiss Axio observer or Leica DM4B (bright field) and Leica SP8 (fluorescence).

Endoscopy

Mice were anaesthetized using an intraperitoneal injection of Nembutal, and a high-resolution mini-endoscope (R. Wolf) was used to determine the mouse endoscopic conditions.

Western blots

Cell lysates from isolated crypts were prepared as previously described[28]. Images were taken using an azure biosystems c280. Crypts were lysed by RIPA and then the insoluble fractions that remained were resuspended by RIPA solution of 6 M urea. The final residue was dissolved in 1× SDS loading buffer.

Dot blot

Purified RNA was used to examine dsRNA, as previously described[29]. A total of 2 μg RNA extracted from 4-dpi small-intestinal crypts of *Setdb1*$^{fl/fl}$ or *Setdb1*$^{iIEC\text{-}KO}$ mice treated with mock or RNase III were dotted on Hybond N+ membranes and immunoblotted with dsRNA-specific J2 antibody.

Quantitative PCR with reverse transcription

Total RNA was extracted from purified crypts, intestinal lamina propria, organoids or single cells isolated by fluorescence-activated cell sorting (FACS), using trizol reagent (Life Technologies), and reverse transcribed into cDNA with the GoScript Reverse Transcription System (Promega). qPCR (ChamQ Universal SYBR qPCR Master Mix, Vazyme) was performed using the CFX Connect Real-Time PCR Detection System (Bio-Rad). Detailed information about the primers used for mouse gene sequences is supplied in Supplementary Table 1.

Immunoprecipitation

Freshly isolated crypts were resuspended and lysed with immunoprecipitation buffer. After centrifuging at 13,000 rpm for 10 min at 4 °C, protein A and G beads were added to the supernatant to prehybridize at 4 °C for 1 h. Anti-ZBP1 antibody was added to the supernatant to rotate for incubation at 4 °C overnight. Then protein A and G beads were added and rotated for 2 h at 4 °C. The beads were washed with immunoprecipitation buffer 8 times at 4 °C and then mixed with an equal volume of 2× SDS sample buffer for western blot.

TEM

Freshly isolated crypts were fixed by 2.5% glutaraldehyde in PBS immediately. After embedding in Epon Araldite, ultrathin sections were cut and analysed using a Hitachi HT-7800 TEM.

IHC intensity of human sections and mouse intestinal length analysis

All human IHC slides were scanned using a Leica Aperio Versa 200 to generate high-content and -resolution digital images. The expression of SETDB1 protein was scored and quantified as previously described[30]. In brief, a multiplicative index of the average staining intensity (0–3) and extent of staining (0–3) in the crypts yields a 10-point staining index that ranged from 0 (no staining) to 9 (extensive, strong staining). For γH2AX, the amount of staining (0–3) in the crypts yields a 4-point staining index that ranged from 0 (no staining) to 3 (extensive, strong staining). Spearman correlation coefficients were used to evaluate the relationships between SETDB1 and γH2AX in 23 SETDB1-low (0–3) or -medium (3–6) patients. For crypts and villi analysis, a total of 50 intact ileal crypts and ileal villi were scaled by Photoshop CS5 and rescaled to MUT/WT as relative length.

Flow cytometry analysis

Crypts from *Lgr5-eGFP-IRES-creERT2;Setdb1*$^{fl/fl}$ mice were isolated[31]. GFP^{high}CD24^{low} ISCs were sorted by FACS (MoFlo Astrios EQS, Beckman Coulter); the sorting strategy is included in Supplementary Fig. 6.

Sorting efficiency was checked under a Leica SP8 confocal instrument (data not shown).

Isolation of crypts and culture of intestinal organoids

Small-intestinal crypts were isolated as previously described[32], with slight modifications. In brief, 10-cm small intestines were cut into 2 pieces and incubated in cold PBS containing 4 mM EDTA for 1 h on ice without shaking. Intestines were then shaken to isolate crypts and filtered through a 70-μm strainer and centrifuged at 400*g* for 5 min to gather crypts. Then, single cells and broken fragments were expelled by centrifuging twice at 400*g* for 25–30 s to get purified crypts. For intestinal organoid culture, crypts were cultured in ENR medium or WENR medium (advanced DMEM/F12 supplemented with B27, N2, EGF and 10% conditioned medium from HEK293T cells expressing Noggin or R-spondin 1 with or without WNT3A) with Matrigel. Primary crypts were allowed to grow for 12 h and then treated with 200 nM 4-OHT for 24 h and removed. For ISC-derived spheroid experiments, 500 cells were plated in a 96-well plate, treated with EtOH or 200 nM 4-OHT for 24 h and then removed and 2 d later clones were counted (3 dpi). If not noted, the medium was changed every 2 d and organoids were shot and collected 2 d after 4-OHT induction (4 dpi). zVAD-fmk (10 μM, stock solution 100 mM resolved in DMSO), Nec-1 (30 μM, stock solution 300 mM resolved in DMSO), GSK'872 (2 μM, stock solution 20 mM resolved in DMSO) and TNF neutralization antibody (20 μg/ml, stock solution 10 mg/ml) were added into organoid growth medium the same time with 4-OHT, and the medium was changed every day; images were taken on the indicated days. Gradient IFNB1 and IFNAR blocking antibodies (10 μg/ml, stock solution 10 mg/ml) were used as indicated in Extended Data Fig. 7f, g.

Lentivirus production and ZBP1-reconstituted organoids

Lentivirus vector of pCDH-MCS-T2A-CopGFP-MSCV was produced according to the manufacturer's instructions (System Biosciences, CD500B-1 – CD523A-1). The ZBP1 N-terminal DNA/RNA binding domain (Zα) truncation, RHIM domain mutation (IQIG to AAAA), and full-length ZBP1 were each cloned to a pCDH vector. Purified crypts were cultured first in WENR medium supplemented with Y-27632 (Sigma) and nicotinamide (Sangon Biotech) for 4 d to enrich ISCs. Then, organoids were trypsinized into single cells and infected with ZBP1 lentivirus or control virus[33]. In brief, single cells mixed with virus were spinoculated in 400*g* and 20 °C for 1 h and then plated in culture incubator for 6 h with WENR medium supplemented with Y-27632, nicotinamide and 8 μg/ml polybrene. After infection, cells were reseeded to grow for 4 d. The spheroids were a snapshot for counting the percentage of GFP$^+$ spheroids, before being trypsinized again into single cells for *Setdb1* deletion by 12 h of treatment with 200 nM 4-OHT. Three days after reseeding, a snapshot of spheroids was taken again for counting the percentage of GFP$^+$ spheroids.

Cross-link immunoprecipitation

Small-intestinal crypts were isolated as described[32]. For cross-link immunoprecipitation (CLIP), cells were overlaid with 3 ml PBS and crosslinked with 150 mJ/cm^2(254 nm) (CX-2000, analytik Jena). Cells were lysed for 30 min in 1 ml RIPA buffer (50 mM Tris-HCl pH 8.0; 15 0mM NaCl; 1% NP-40; 0.1% SDS; 0.5% deoxycholate; 2 mM EDTA). Lysates were added with 12.5 μl RNasin Plus (Promega). Lysates were centrifuged for 15 min at 12,000rpm and 50 μl supernatant was used as input. Samples were incubated with 6 μg of anti-ZBP1 and IgG overnight at 4 °C. Antibody was immunoprecipitated with 80 μl protein A and G plus agarose beads (Millipore). After 3 h, beads were washed twice with high-salt wash buffer (50 mM Tris-HCl pH 8.0; 500 mM NaCl; 1% NP-40; 0.1% SDS; 0.5% deoxycholate) and once with RIPK buffer. Beads were resuspended in 100 μl of reverse buffer (100 mM Tris-HCl pH8.0; 10 mM EDTA; 1% SDS;100 mM DTT) with 10 μl 5M NaCl and 50 μg proteinase K. Beads were then incubated in a heating block at 4 2 °C for 1 h to digest peptide, and 65 °C for 1.5 h to reverse the crosslink. The trizol method was used to extract total RNA. Finally, purified RNA was used to examine dsRNA, as previously described[29].

Image acquisition and analysis of organoid cell death

For the propidium-iodide (PI)-traced organoid cell-death assay, organoids were stained with 1 μg/ml PI after removal of 4-OHT and images were taken using a ZEISS Axio observer, the percentage of PI and organoid area was calculated by Photoshop CS5.

Administration of antibiotics

Antibiotics were administered as previously described[34]. Ciprofloxacin hydrochloride (0.2 mg/ml), ampicillin sodium salt (1 mg/ml), metronidazole (1 mg/ml), vancomycin hydrochloride (0.5 mg/ml) and kanamycin sulfate (0.5 mg/ml) were dissolved in sterile water. Mice involved in the experiment were pretreated with antibiotics water two weeks ahead of induction. During the experiment, all instruments and reagents were refreshed every other day. All of experiment instruments were sterilized at high temperature and pressure before use.

GSK'872 administration

First, 2 mg/ml GSK'872 was dissolved in solvent. The solvent comprised 2% DMSO, 2% Tween-80, 35% PEG-300 and sterile water. Mice received 10 μl/g solvent as control or solvent with GSK'872, by intraperitoneal injection every 2 d, from the start of the experiment until death.

Transcriptome RNA sequencing and analysis

Purified total RNA from *Setdb1*$^{fl/fl}$ and *Setdb1*$^{iIEC\text{-}KO}$ crypts was used for RNA-sequencing (RNA-seq) preparation. cDNA library construction and sequencing were performed by Beijing Genomics Institute using a BGISEQ-500 sequencer. At least 21 million clean reads were aligned to the mouse genome (mm10) by HISAT2. Then, the gene-expression level of each sample was calculated with RSEM. On the basis of the gene-expression level, the differentially expressed genes were detected by DEGseq and PossionDis algorithms. The *P* value was calculated by PossionDis[35]. Differentially expressed genes were defined as genes with a false discovery rate of less than 0.001 and fold change larger than 2. We performed pathway functional enrichment using phyper, a function of R, and the *P* value was calculated.

RNA-seq for repeats and analysis

ISC-related RNA-seq was performed in-house. Total RNA was extracted from GFP^{high}CD24^{low} ISCs from *Lgr5-eGFP-IRES-creERT2;Setdb1*$^{fl/fl}$ mice (corn-oil-treated, $n = 3$; tamoxifen-treated, $n = 9$) 5 d after the first gavage. After depletion of ribosomal RNA, a strand-specific cDNA library was constructed by Beijing Genomics Institute, and then subjected to sequencing with Illumina HiSeq X-ten. The 150-bp paired-end raw reads were qualified and cleaned by fastp with default settings[36]. Clean reads were mapped onto the mouse genome (GRCm38/mm10) using HISAT2 to obtain the aligned .bam files[37]. The annotation file of mouse ERVs was generated by RepeatMasker v.4.0.7, comparing with Repbase consensus sequences (edition-20181026) and a further-customized ERV .gtf file with high Smith–Waterman scores (≥2,000) was produced as per a previous report[19]. The overlap reads for ERVs were summarized by featureCounts[38] and then quantified by EdgeR with the Benjamini–Hochberg-corrected *P* value < 0.05. Detailed information about repeats is included in Supplementary Table 1. Raw RNA-seq data of repeats of other cells, including B cells[39], immortalized mouse embryonic fibroblasts[19], pro-B cells[40], mouse embryonic stem cells[41] were publically available.

Chromatin immunoprecipitation with sequencing, and analysis

GFP^{high}CD24^{low} ISCs were prepared as described in 'Flow cytometry analysis'. The chromatin immunoprecipitation with sequencing

(ChIP–seq) protocol was performed as previously described[42], with slight modifications. In brief, approximately 3×10^6 cells were cross-linked with 1% formaldehyde for 10 min at room temperature, followed by quenching in 125 nM glycine. Cell nuclei were collected and lysed in lysing buffer (50 mM HEPES/KOH pH 7.6, 1 mM EDTA, 140 nM NaCl, 10% v/v glycerol, 0.5% NP-40, 0.25% v/v Triton X-100) supplemented with protease inhibitor. Nuclei were subjected to sonication to acquire DNA fragments of 200–350 bp in size. The sonicated chromatin was applied to immunoprecipitation by incubation with H3K9me3 antibody overnight at 4 °C, followed by collection using 50 μl protein A and G plus agarose beads (Millipore). Subsequent processes were implemented according to the protocol. The ChIP–seq library was prepared using a KAPA HyperPrep Kit (Roche, 07962347001), according to the manufacturer's instructions. Library concentrations were mixed equally for sequencing at Hiseq-Xten to generate 150-bp reads from paired-ends. The analysis of ChIP–seq data was performed as previously described[43]. In brief, after quality assessment by fastp, clean reads were aligned to the mouse genome (GRCm38/mm10) using Bowtie2 (version 2.2.8). Enriched peaks of H3K9me3 were identified by HOMER v.4.10.1 with histone style (http://homer.ucsd.edu/homer). The aligned H3K9me3 .bam file was converted into a .bigwig file and processed to plot the H3K9me3 density on the ERVs of interest using deepTools2.0.

Statistical analysis

Data shown in graphs are mean ± s.e.m., except for mouse weight curves, which are mean ± s.d. All values are calculated from at least three independent biological replicates, unless specifically stated. In all tests (except survival curves), the two-tailed unpaired *t*-test was used; survival curves were conducted under log–rank test and a 95% confidence interval was used. Statistical analysis was performed using GraphPad Prism 8, SPSS 19 and Microsoft Excel 2017.

Reporting summary

Further information on research design is available in the Nature Research Reporting Summary linked to this paper.

Data availability

The datasets generated during the current study are available in the GEO database, with the accession code GSE129174. All other data generated in this Article are provided in the Supplementary Information and Source Data; Source Data for Figs. 1–4 and Extended Data Figs. 1–9 are provided with the paper. The *Setdb1*$^{fl/fl}$ mice are available from the corresponding authors upon request.

26. Zhang, K. et al. *In vitro* expansion of primary human hepatocytes with efficient liver repopulation capacity. *Cell Stem Cell* **23**, 806–819.e4 (2018).
27. Mo, W. et al. CXCR4/CXCL12 mediate autocrine cell-cycle progression in NF1-associated malignant peripheral nerve sheath tumors. *Cell* **152**, 1077–1090 (2013).
28. Mo, W. et al. Nuclear β-arrestin1 functions as a scaffold for the dephosphorylation of STAT1 and moderates the antiviral activity of IFN-γ. *Mol. Cell* **31**, 695–707 (2008).
29. Sheng, W. et al. LSD1 ablation stimulates anti-tumor immunity and enables checkpoint blockade. *Cell* **174**, 549–563.e19 (2018).
30. Liu, Y. et al. Epithelial EZH2 serves as an epigenetic determinant in experimental colitis by inhibiting TNFα-mediated inflammation and apoptosis. *Proc. Natl Acad. Sci. USA* **114** E3796–E3805 (2017).
31. Sato, T. et al. Single Lgr5 stem cells build crypt–villus structures *in vitro* without a mesenchymal niche. *Nature* **459**, 262–265 (2009).
32. Yuan, H. et al. Histone methyltransferase SETD2 modulates alternative splicing to inhibit intestinal tumorigenesis. *J. Clin. Invest*. **127**, 3375–3391 (2017).
33. Andersson-Rolf, A., Fink, J., Mustata, R. C. & Koo, B. K. A video protocol of retroviral infection in primary intestinal organoid culture. *J. Vis. Exp*. **90**, e51765 (2014).
34. Takahashi, N. et al. RIPK1 ensures intestinal homeostasis by protecting the epithelium against apoptosis. *Nature* **513**, 95–99 (2014).
35. Audic, S. & Claverie, J. M. The significance of digital gene expression profiles. *Genome Res*. **7**, 986–995 (1997).
36. Chen, S., Zhou, Y., Chen, Y. & Gu, J. fastp: an ultra-fast all-in-one FASTQ preprocessor. *Bioinformatics* **34**, i884–i890 (2018).
37. Kim, D., Langmead, B. & Salzberg, S. L. HISAT: a fast spliced aligner with low memory requirements. *Nat. Methods* **12**, 357–360 (2015).
38. Liao, Y., Smyth, G. K. & Shi, W. featureCounts: an efficient general purpose program for assigning sequence reads to genomic features. *Bioinformatics* **30**, 923–930 (2014).
39. Collins, P. L., Kyle, K. E., Egawa, T., Shinkai, Y. & Oltz, E. M. The histone methyltransferase SETDB1 represses endogenous and exogenous retroviruses in B lymphocytes. *Proc. Natl Acad. Sci. USA* **112**, 8367–8372 (2015).
40. Pasquarella, A. et al. Retrotransposon derepression leads to activation of the unfolded protein response and apoptosis in pro-B cells. *Development* **143**, 1788–1799 (2016).
41. Karimi, M. M. et al. DNA methylation and SETDB1/H3K9me3 regulate predominantly distinct sets of genes, retroelements, and chimeric transcripts in mESCs. *Cell Stem Cell* **8**, 676–687 (2011).
42. Liu, Z. et al. Nucleoporin Seh1 interacts with Olig2/Brd7 to promote oligodendrocyte differentiation and myelination. *Neuron* **102**, 587–601.e7 (2019).
43. Lu, X. et al. Multiple P-TEFbs cooperatively regulate the release of promoter-proximally paused RNA polymerase II. *Nucleic Acids Res*. **44**, 6853–6867 (2016).

Acknowledgements We thank L. Hui, Y. Chen, J. Qin and Y. Nie for experimental resources, and L. Yao for technical support. The study was supported by the National Natural Science Foundation of China (81788101 to J. Han, 81472725 to W.M., 31971329 and 31501096 to M.L., and 81602675 to J. Hu), the Fundamental Research Funds for the Central Universities (20720160072 and 20720190086 to W.M.).

Author contributions R.W., H.L., J. Han and W.M. designed experiments, performed data analyses and wrote the manuscript. R.W., H.L., Y.L., H.N., Z.-Y.C., Z.-H.Y. and W.L. performed experiments. B.L., H.C., X.Q. and P.L. provided specimens from patient with IBD. J.W. provided relevant mice. R.W., H.L., Z.-Y.C., J. Hu, Y.L. and M.L. performed biochemical analysis of *Setdb1*-deficient mice. W.M. supervised the study.

Competing interests The authors declare no competing interests.

Additional information
Supplementary information is available for this paper at https://doi.org/10.1038/s41586-020-2127-x.
Correspondence and requests for materials should be addressed to J.H. or W.M.
Peer review information *Nature* thanks Alexander N. Poltorak and the other, anonymous, reviewer(s) for their contribution to the peer review of this work.
Reprints and permissions information is available at http://www.nature.com/reprints.

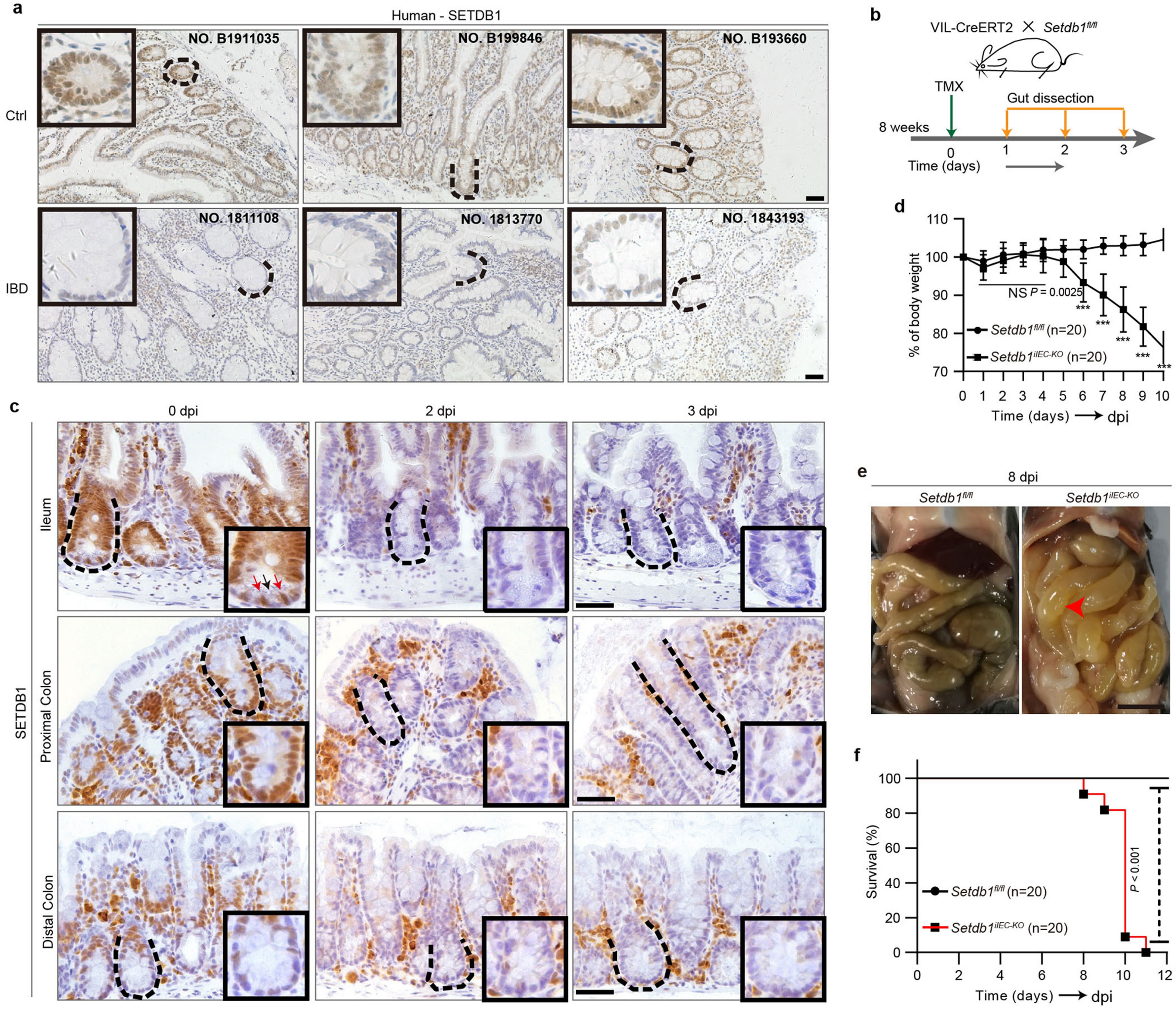

Extended Data Fig. 1 | Mouse model to mimic SETDB1 inactivation in patients with IBD. **a**, SETDB1 IHC of human surgical samples; data are related those in Fig. 1d. Insets show high magnifications of crypts. The complete set of images is included in Supplementary Fig. 2 ($n = 17$). $n = 30$ samples from patients with IBD. **b**, Mouse model and work flow. One dose of tamoxifen was used. **c**, Left, SETDB1 IHC in mouse ileal and colonic sections. SETDB1 is highly expressed in ISCs (inset in top panel; red arrows) and is absent in the Paneth cell (inset in top panel, black arrow). Middle and right, SETDB1 disappears in epithelial cells (dotted line and insets) and remains in non-epithelial cells. At least three sections were taken each day with similar results. **d**, Body weight curves of *Setdb1$^{fl/fl}$* and *Setdb1$^{iIEC\text{-}KO}$* mice after tamoxifen induction ($n = 20$ mice). *P* values and significance were determined by a two-sided unpaired *t*-test, $^{***}P < 0.001$. **e**, Anatomy images of 8-dpi intestine of *Setdb1$^{fl/fl}$* and *Setdb1$^{iIEC\text{-}KO}$* mice after tamoxifen induction. Red arrow shows signs of watery diarrhoea; $n = 3$ mice were repeated. **f**, Kaplan–Meier survival curves of *Setdb1$^{fl/fl}$* and *Setdb1$^{iIEC\text{-}KO}$* mice after tamoxifen induction ($n = 20$ mice), *P* values were determined by log–rank test, 95% confidence interval of ratio. Scale bars, 50 µm. Data are mean ± s.e.m.

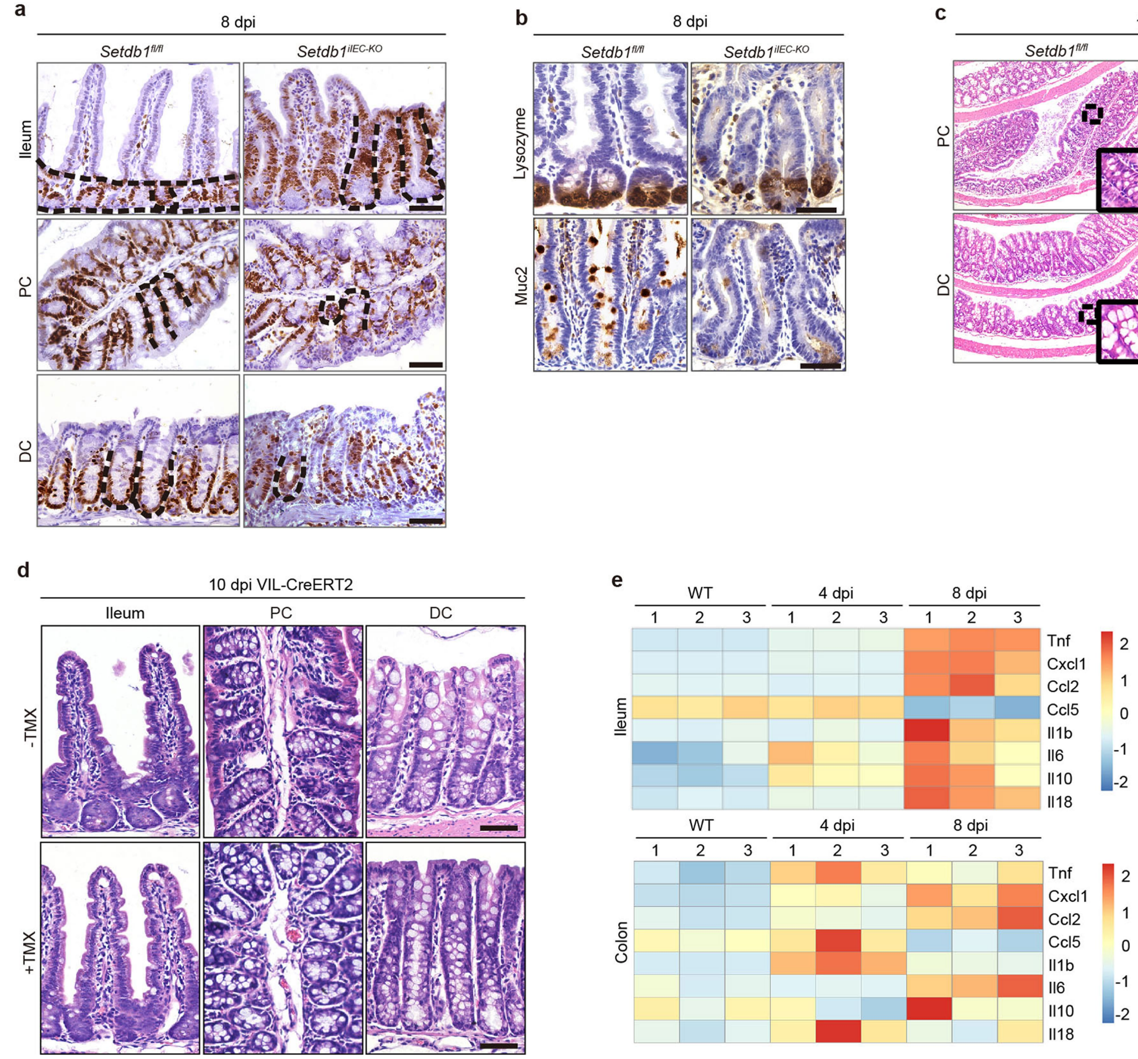

Extended Data Fig. 2 | Dysplasia and inflammation occur after *Setdb1* deletion in the mouse intestine. a, Ki67 staining of ileum and colon of mice at 8 dpi (*n* = 6 mice). **b**, Lysozyme (Paneth cells) and MUC2 (goblet cells) of ileum of mouse at 8 dpi (*n* = 6 mice). **c**, H & E staining revealed a considerable breakdown of the colonic epithelium barrier at 10 dpi in mice of the indicated genotypes. Insets are magnified crypts, showing crypt destruction and colitis (*n* = 3 mice). **d**, H & E images of VIL–CreERT2 mice induced with or without tamoxifen, *n* = 3 mice were repeated with no difference between two groups. **e**, Heat map of chemokines and interleukins in ileal and colonic lamina propria of 4-dpi and 8-dpi mice (*n* = 3 mice). Scale bars, 50 µm. Data are mean ± s.e.m.

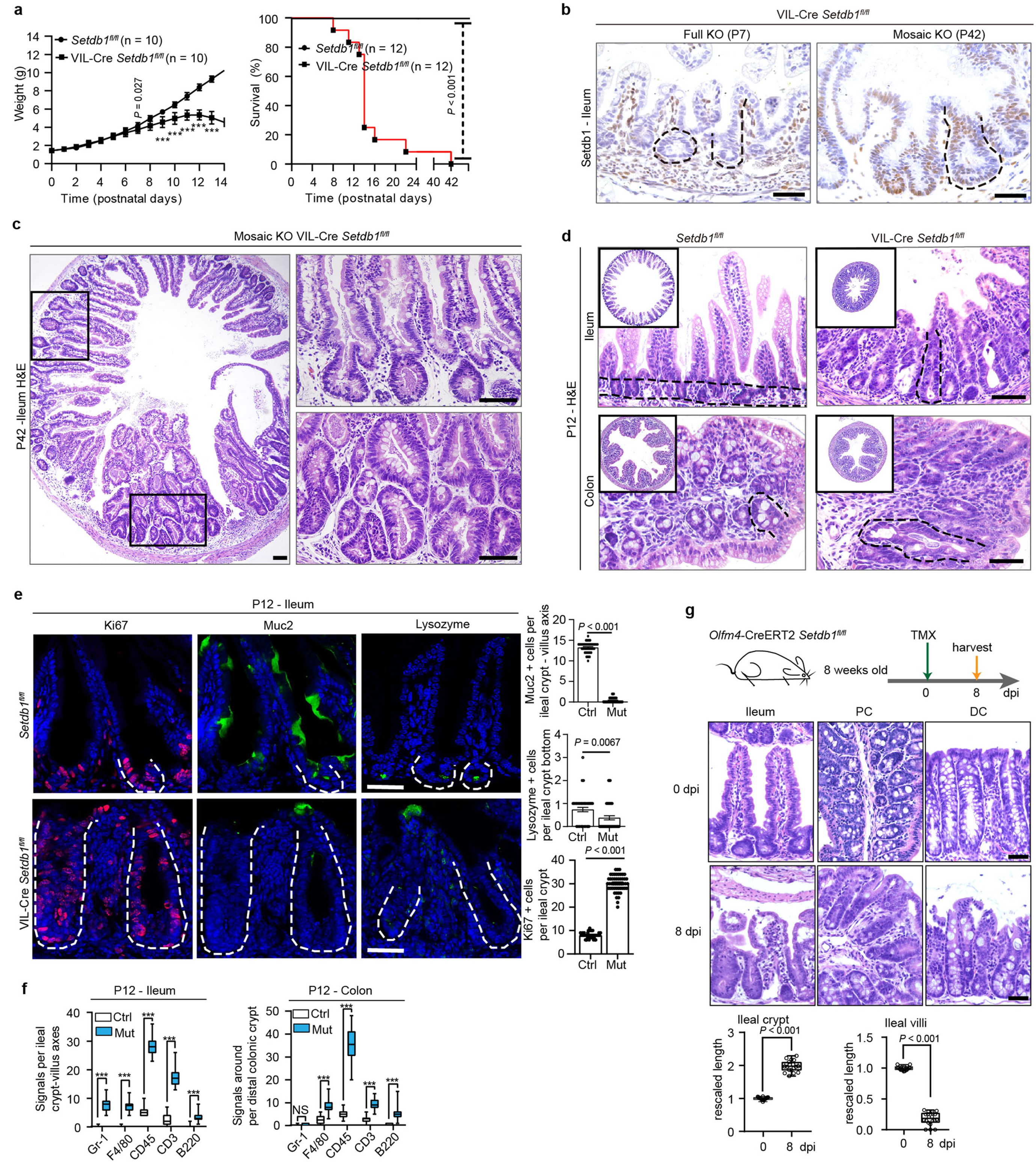

Extended Data Fig. 3 | See next page for caption.

Extended Data Fig. 3 | VIL–Cre *Setdb1*$^{fl/fl}$ mice and mice with *Setdb1* deleted specifically in ISCs also show inflammatory symptoms. a, Weight ($n = 10$ mice of each genotype) and Kaplan–Meier survival curves ($n = 12$ mice of each genotype) of *Setdb1*$^{fl/fl}$ and VIL–Cre *Setdb1*$^{fl/fl}$ mice. The weight curve was determined by two-tailed *t*-test. *P* value of survival curve was determined by log–rank test, 95% confidence interval of ratio. **b**, Representative images of SETDB1-knockout efficacy of VIL–Cre *Setdb1*$^{fl/fl}$ mice (full knockout (KO), $n = 6$ mice; mosaic knockout, $n = 2$ mice were found). Dotted lines in the left panel denote that no SETDB1 expressed. Dotted lines in the right panel demonstrate that most of the cells expressed SETDB1; adenomas shown in **c** share a similar SETDB1 expression pattern, as they came from the same paraffin block. **c**, H & E staining of *Setdb1* mosaic-knockout mice (postnatal day (P)42) developed aberrant crypts (top inset) and adenomas (bottom inset). $n = 2$ mice. **d**, H & E staining of *Setdb1* full-knockout mice at P12 ($n = 6$ mice). Insets show the thin bowel and narrowed lumen of *Setdb1* full-knockout mice. Dotted lines depict crypts. **e**, Staining for Ki67 (proliferative cells), lysozyme (Paneth cells) and MUC2 (goblet cells) from P12 ileal sections, as indicated. $n = 50$ crypt–villus axes. At least three individual experiments were performed and cells were counted, with similar results. **f**, Lymphocyte IHC signals in ileum or colon. $n = 50$ crypt–villus axes. Three individual experiments were performed with similar results. Box plots show median and 25th to 75th percentiles, and whiskers indicate the minimum and maximum values. **g**, Inflammatory bowel damage in *Olfm4-creERT2;Setdb1*$^{fl/fl}$ mice. H & E staining at 0 dpi and 8 dpi was compared (20 crypts or villi were counted). Scale bars, 50 µm. Data are mean ± s.e.m. Box plots show median and 25th to 75th percentiles, and whiskers indicate the minimum and maximum values. *P* values and significance were determined by two-sided unpaired *t*-test. NS, not significant; $^{***}P < 0.001$.

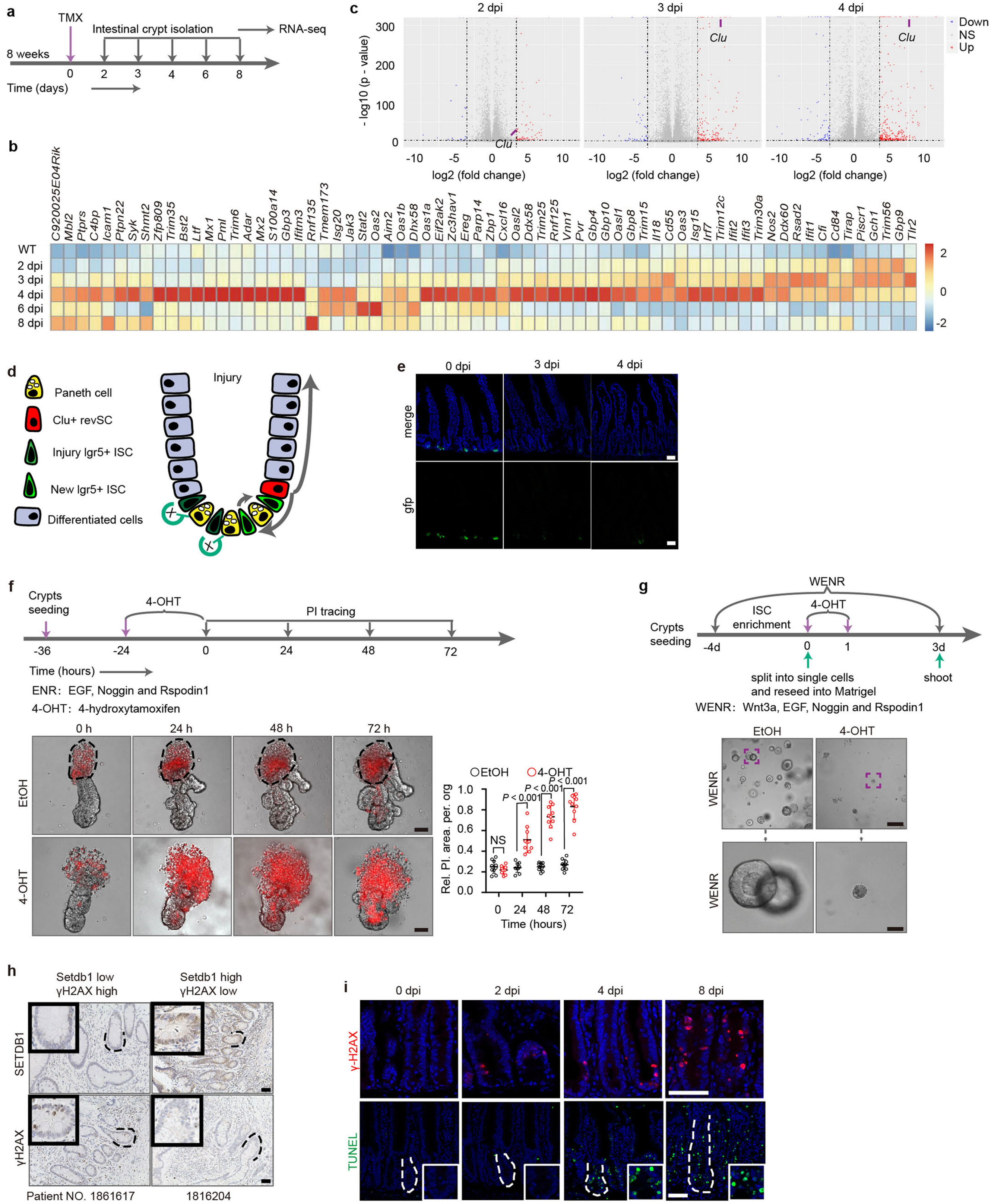

Extended Data Fig. 4 | See next page for caption.

Extended Data Fig. 4 | SETDB1 deficiency activates innate immunity and ISC death. **a**, Schematic of RNA-seq. **b**, Heat map depiction of innate-immunity-related genes. **c**, Volcano plot of differentially expressed genes ($\log_2$-transformed fold change ≥ 3.5 or ≤ −3.5; *P* value < 0.001) at 2, 3 and 4 dpi. *n* = 1 mouse for each day. Details of statistical analysis are provided in Methods. **d**, Scenario of CLU$^+$ revival stem cells (revSCs) for ISC injury. Revival stem cells are very rare under homoeostasis, but expanded rapidly upon injury of LGR5$^+$ ISCs to regenerate the intestine. **e**, Representative images show GFP$^+$ cells after tamoxifen induction in *Lgr5-eGFP-* *Setdb1$^{iIEC\text{-}KO}$* mice. **f**, PI-traced organoids from VIL−CreERT2 *Setdb1$^{fl/fl}$* mice treated with EtOH as control or 4-OHT to induce *Setdb1* deletion (four individual experiments were performed with similar results). Panel to the right of the images is a statistical analysis of the relative PI area per organoid (*n* = 10 organoids). **g**, Images of single ISC-derived spheroids in WENR medium. Experiment was repeated three times, with similar results. **h**, Representative images of lower SETDB1 IHC intensity correlating with higher γH2AX IHC intensity. The complete set of images of γH2AX and SETDB1 IHC is provided in Supplementary Fig. 2. *n* = 23 samples. **i**, Representative images of γH2AX and TUNEL staining, *n* = 3 experimental repeats for each day. Scale bars, 50 μm. Data are mean ± s.e.m. *P* values were determined by two-sided unpaired *t*-test.

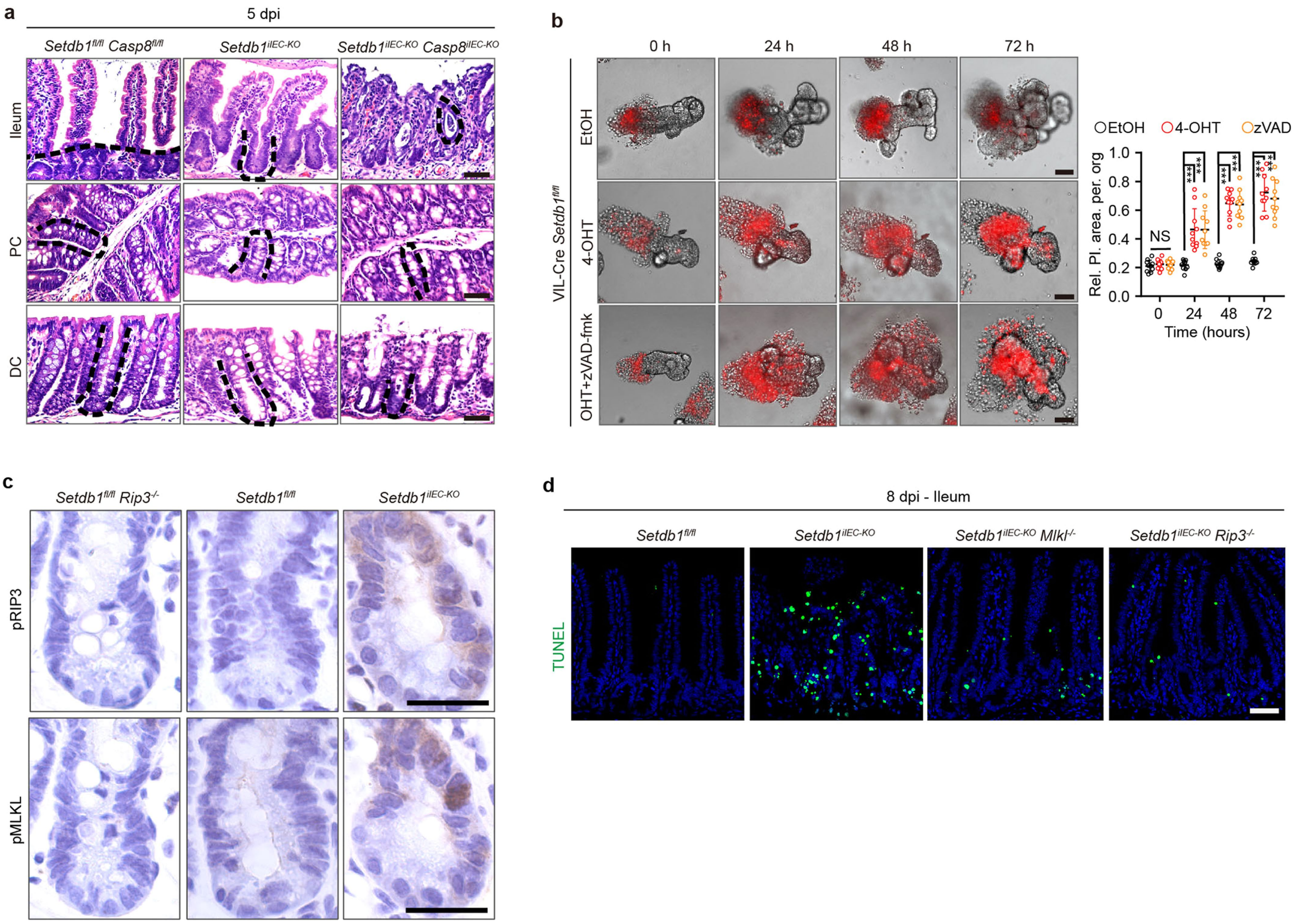

Extended Data Fig. 5 | Apoptosis blockade does not rescue cell death by *Setdb1* deletion in vivo and ex vivo. a, H & E staining of ileum and colon from mice of different genotypes (as indicated) at 5 dpi. $n = 3$ mice. **b**, Microscopy image of PI-stained organoids. The panel to the right of the images is a statistical analysis of the relative PI area per organoid ($n = 10$ organoids). **c**, IHC staining of pRIP3 and pMLKL of ileal crypts (at 6 dpi) from continuous paraffin sections. $n = 3$ mice. **d**, Representative images of TUNEL signals in crypts. Experiment was performed on $n = 3$ mice individually, with similar results. Scale bars, 50 µm (**a**, **b**, **d**), 25 µm (**c**). Data are mean ± s.e.m. Significance was determined by two-sided unpaired t-test. NS, not significant; $^{***}P < 0.001$.

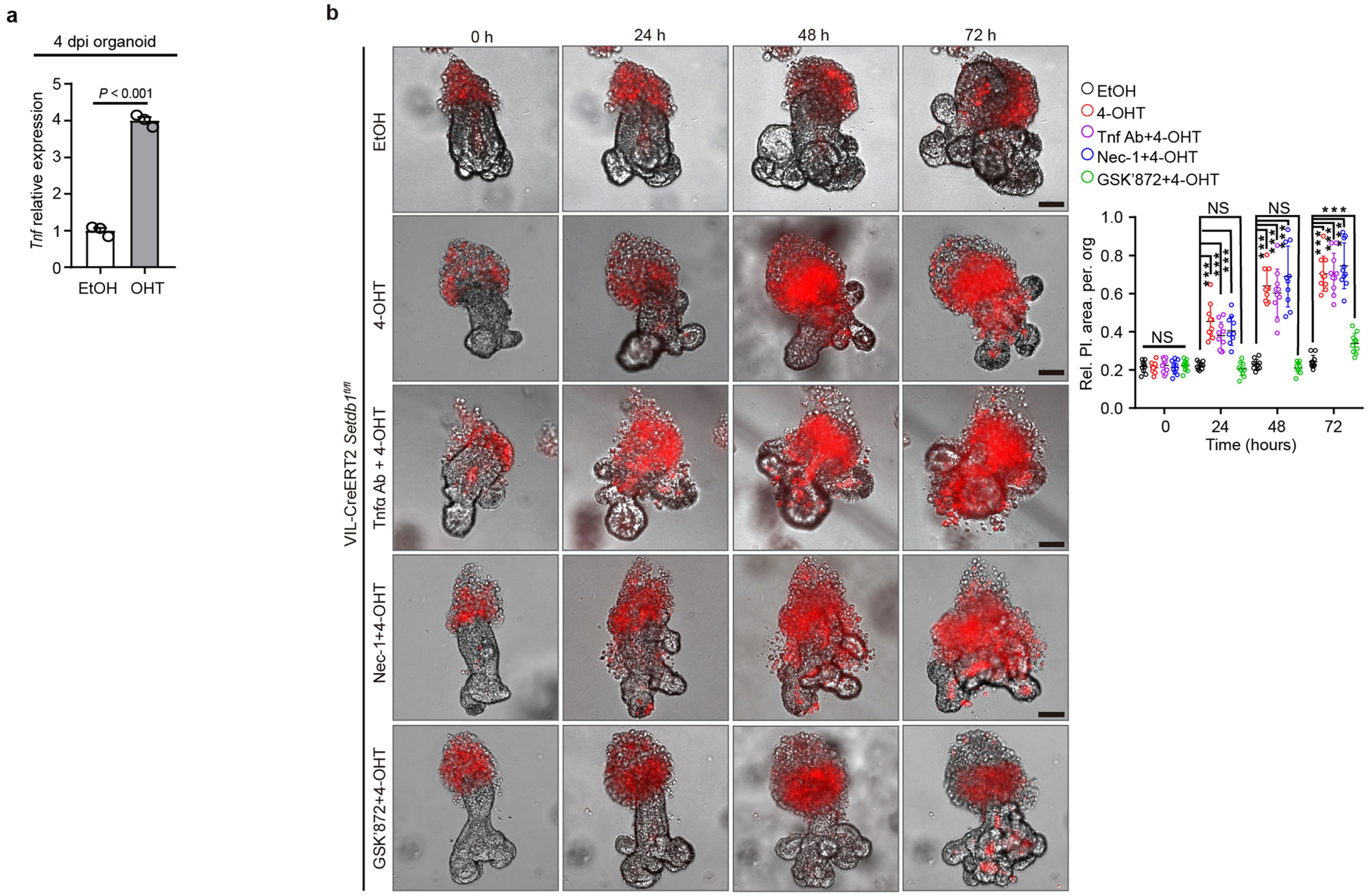

Extended Data Fig. 6 | RIP1-kinase-independent necroptosis contributes to cell death in *Setdb1*-null organoids. a, qPCR with reverse transcription of *Tnf* (*n* = 3 experimental repeats). **b**, Organoids from VIL–CreERT2 *Setdb1*$^{fl/fl}$ mice were treated with TNF neutralizing antibody, Nec-1 (RIP1-kinase inhibitor) or GSK'872 (RIP3-kinase inhibitor) with or without 4-OHT, as indicated. The panel to the right of the images is a statistical analysis of the relative PI area per organoid (*n* = 10 organoids). Three individual experiments were performed, with similar results. Scale bars, 50 µm. Data are mean ± s.e.m. *P* values were determined by two-sided unpaired *t*-test. NS, not significant; ***$P < 0.001$.

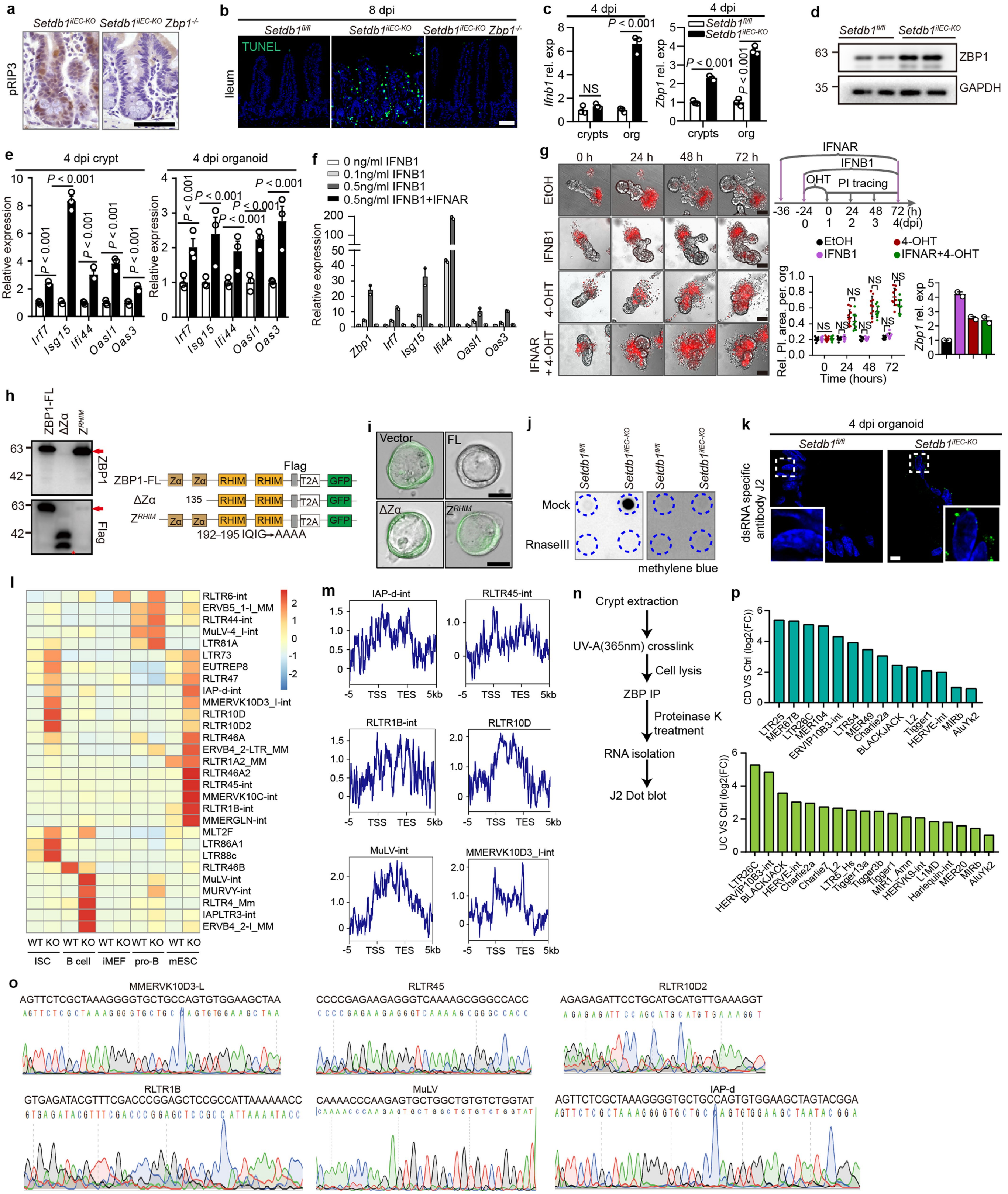

Extended Data Fig. 7 | See next page for caption.

Extended Data Fig. 7 | ZBP1 can be induced by IFN but the initiation of necroptosis by ZBP1 requires ERVs. a, IHC staining of pRIP3. Data shown are related to those in Fig. 4b. $n = 3$ mice. **b**, TUNEL staining of ileum from mice of different genotypes (as indicated) at 8 dpi. Data shown are related to those in Fig. 4c. $n = 3$ mice. **c**, qPCR of *Ifnb1* and *Zbp1* expression in 4-dpi small-intestinal crypts and organoids. $n = 3$ experimental repeats. **d**, Immunoblot of ZBP1 from 4-dpi small-intestinal crypts. $n = 2$ mice. **e**, qPCR of expression of interferon-stimulated genes. $n = 3$ experimental repeats. **f**, qPCR of relative expression of interferon-stimulated genes in *Setdb1* wild-type organoids treated as indicated. $n = 2$ experimental repeats. **g**, Representative images of PI-traced organoids. The procedure of the treatments with 0.1 ng ml^{-1} IFNB1, 10 μg ml^{-1} IFNAR and 200 nM 4-OHT is shown to the right of the top panel. The bottom panel to the right of the images shows the statistics of relative PI area per organoid ($n = 10$ organoids). The bottom panel on the far right shows ZBP1 expression level. $n = 2$ experimental repeats. **h**, Truncated and mutated ZBP1, as used in Fig. 4h. The expressions of full-length ZBP1 (ZBP1-FL) and ZBP1(RHIM) (Z^{RHIM}) were confirmed by anti-ZBP1 antibody (sc-271483) raised against amino acids 1–300 of mouse ZBP1, whereas ZBP1(ΔZα) was confirmed by anti-Flag antibody. The asterisk marks a specific band of ΔZα. The experiment was repeated three times. **i**, Representative images of GFP^{+} spheroids. These images are related to the right histogram of Fig. 4h. The experiment was repeated three times. **j**, Dot blot by J2 antibody of dsRNA from 4-dpi intestinal crypts. $n = 3$ experimental repeats. **k**, J2 staining revealed dsRNA enrichment in SETDB1-deprived organoids. $n = 2$ experimental repeats. Scale bars, 5 μm. **l**, RNA-seq for repeats revealed the level of ERVs in different cells, including ISCs, B cells, immortalized myofibroblast (iMEFs), pro-B cells and mouse embryonic stem cell (mESCs). **m**, H3K9me3 intensity profiles on different ERVs in ISCs. Next-generation sequencing plots show the fold of enrichment of H3K9me3 from −5 kb to 5 kb around genomic ERV elements in ISCs. TSS, transcription start site of ERV. TES, transcription end site. **n**, Schematic of CLIP assay. Data are shown in Fig. 4j. **o**, PCR with reverse transcription was performed with RNAs in ZBP1 immunoprecipitated from *Setdb1*-null crypts. The PCR products using specific primers of six ERVs (Fig. 4i) were sequenced (bottom sequences) and aligned to Repbase (top sequences), RNA of 4-dpi crypts from *Setdb1*$^{iIEC\text{-}KO}$ mice. $n = 2$ mice. **p**, Biopsies from patients with IBD and unaffected controls (control, $n = 5$; Crohn's disease (CD), $n = 6$; ulcerative colitis (UC), $n = 4$) show increased virus mimicry repeats in patients with IBD. Scale bars, 50 μm. Data are mean ± s.e.m. P values were determined by two-sided unpaired t-test. NS, not significant ($P > 0.05$).

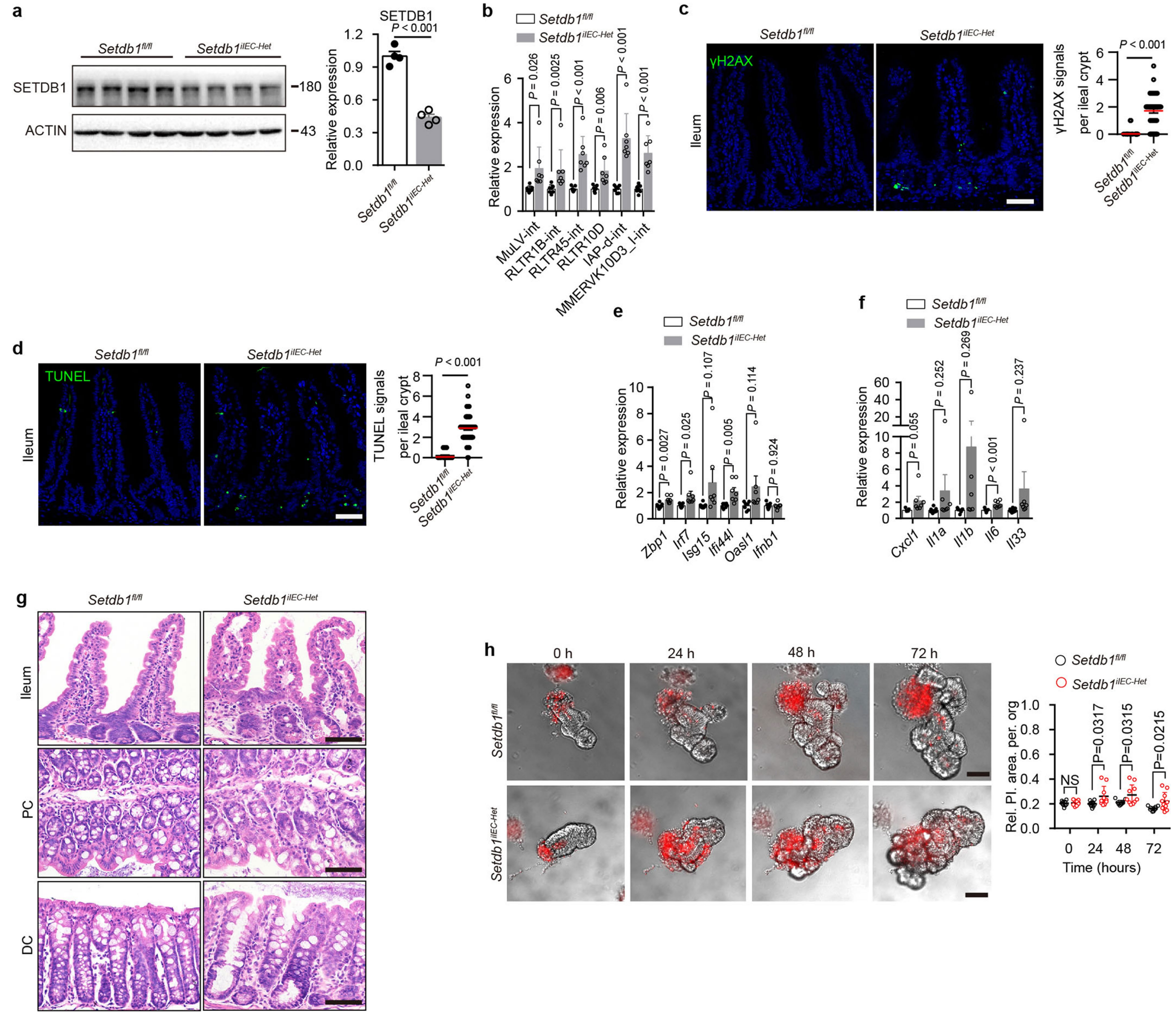

Extended Data Fig. 8 | Bowel inflammation in *Setdb1*$^{iIEC\text{-}Het}$ mice. a, Left, western blot of SETDB1 in 4-dpi crypts. Right, Quantification of western blot intensities ($n = 4$ mice). **b**, qPCR of relative expression of ERVs at 4 dpi, $n = 7$ mice. **c**, Representative immunofluorescence of γH2AX staining in 4-dpi ileal sections. $n = 50$ crypts. Experiments were repeated in three mice. **d**, TUNEL assay of 4-dpi ileal sections. $n = 3$ mice were examined. $n = 50$ crypts. **e**, The expression of genes related to the type-I-interferon pathway in 4-dpi crypts. $n = 7$ mice. **f**, The expression of chemokines and interleukins in 4-dpi crypts. $n = 7$ mice. **g**, H & E staining of 4-dpi intestinal sections, showing destroyed epithelium in *Setdb1*$^{iIEC\text{-}Het}$ mice. $n = 2$ mice were found within 13 mice collected. **h**, PI-traced organoids were counted, out of $n = 10$ organoids were examined in total. Scale bars, 50 μm. Data are mean ± s.e.m. *P* values were determined by two-sided unpaired *t*-test. NS, not significant ($P > 0.05$).

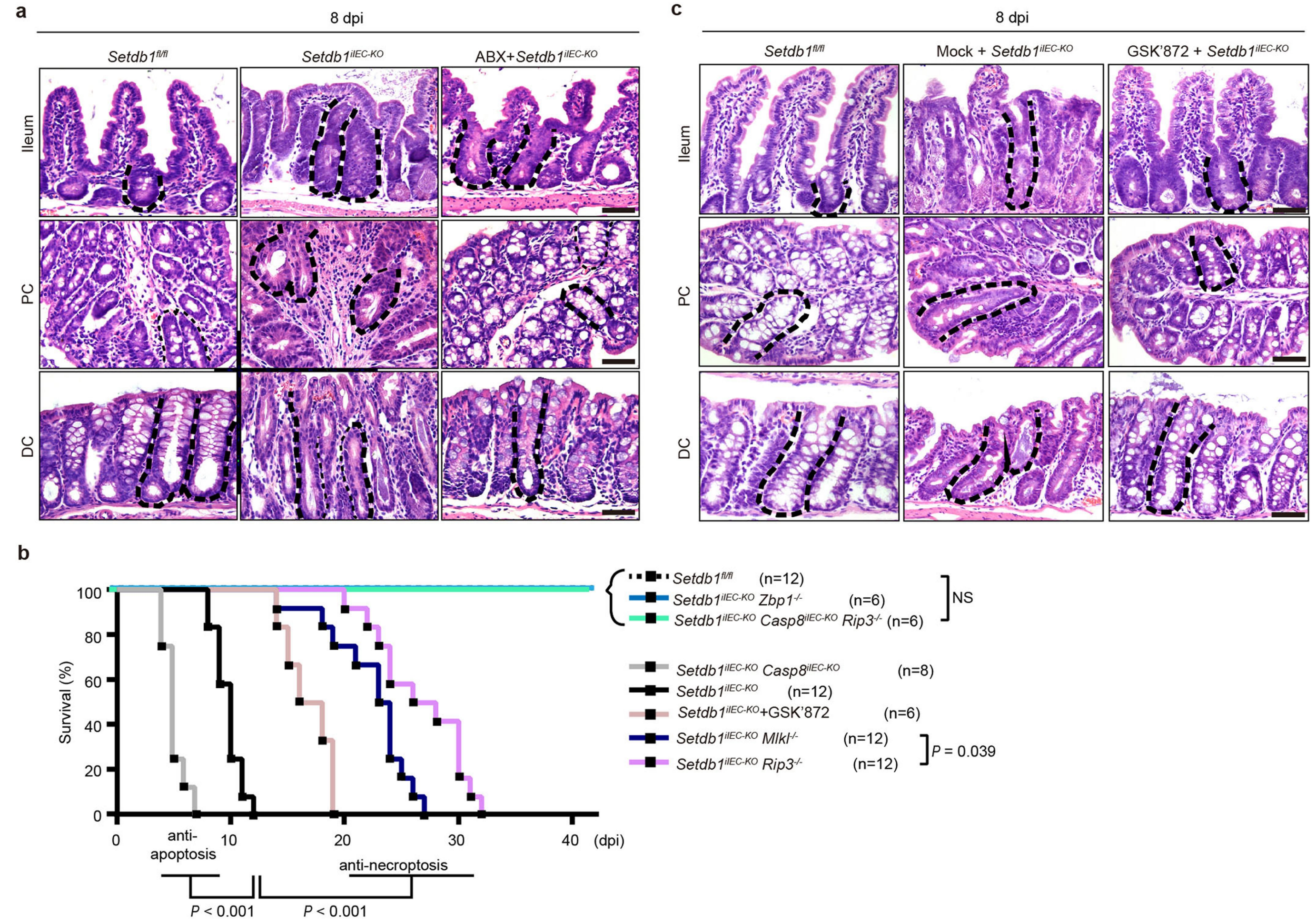

Extended Data Fig. 9 | Necroptosis is the primary cause of death in *Setdb1*$^{iIEC\text{-}KO}$ mice. a, H & E staining of intestine sections at 8 dpi, from *Setdb1*$^{fl/fl}$ and *Setdb1*$^{iIEC\text{-}KO}$ mice treated with or without broad spectrum antibiotics (ABX) as indicated. $n = 3$ mice were collected and checked, with similar results. **b**, Kaplan–Meier survival curves of mice used in this study. **c**, H & E staining of intestine sections at 8 dpi from *Setdb1*$^{fl/fl}$ and *Setdb1*$^{iIEC\text{-}KO}$ mice treated with mock or GSK'872 as indicated. $n = 3$ mice were checked, with similar results. Scale bars, 50 µm. P values were determined by log–rank test, 95% confidence interval of ratio. NS, not significant ($P > 0.05$).

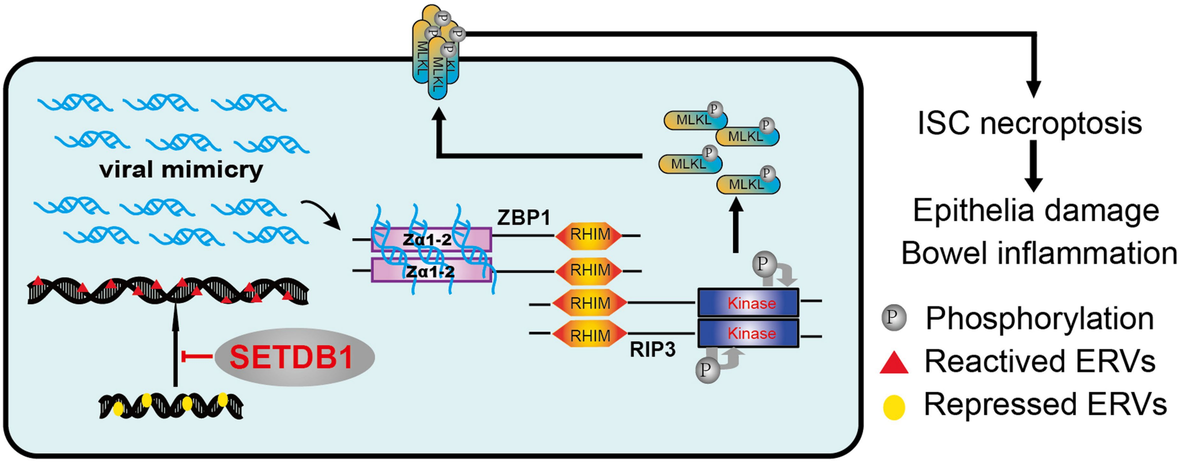

Extended Data Fig. 10 | SETDB1 safeguards genome stability against ZBP1-mediated necroptosis in ISCs. SETDB1 protects genome integrity by enforcing repression of ERVs. Once SETDB1 is dysfunctional, reactive ERVs can produce multiple viral mimicry dsRNAs to activate ZBP1 for RIP3–MLKL necroptosis. Pro-inflammatory necroptosis breaks the epithelial barrier and promotes bowel inflammation.

Extended Data Table 1 | The most-significantly upregulated genes in mutant crypts

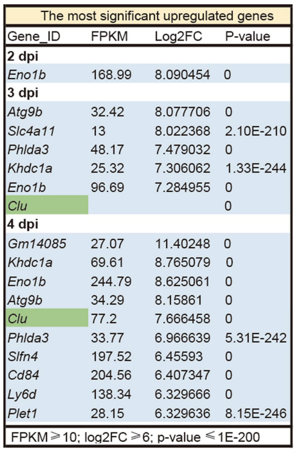

The most significant upregulated genes			
Gene_ID	FPKM	Log2FC	P-value
2 dpi			
Eno1b	168.99	8.090454	0
3 dpi			
Atg9b	32.42	8.077706	0
Slc4a11	13	8.022368	2.10E-210
Phlda3	48.17	7.479032	0
Khdc1a	25.32	7.306062	1.33E-244
Eno1b	96.69	7.284955	0
Clu			0
4 dpi			
Gm14085	27.07	11.40248	0
Khdc1a	69.61	8.765079	0
Eno1b	244.79	8.625061	0
Atg9b	34.29	8.15861	0
Clu	77.2	7.666458	0
Phlda3	33.77	6.966639	5.31E-242
Slfn4	197.52	6.45593	0
Cd84	204.56	6.407347	0
Ly6d	138.34	6.329666	0
Plet1	28.15	6.329636	8.15E-246
FPKM ⩾ 10; log2FC ⩾ 6; p-value ⩽ 1E-200			

Clu was at the top of the list of the most-significantly upregulated genes. For statistical analysis, see ‘Transcriptome RNA sequencing and analysis’ in Methods.

nature research

Corresponding author(s): Wei Mo

Reporting Summary

Nature Research wishes to improve the reproducibility of the work that we publish. This form provides structure for consistency and transparency in reporting. For further information on Nature Research policies, see Authors & Referees and the Editorial Policy Checklist.

Statistical parameters

When statistical analyses are reported, confirm that the following items are present in the relevant location (e.g. figure legend, table legend, main text, or Methods section).

n/a	Confirmed	
☐	☒	The exact sample size (*n*) for each experimental group/condition, given as a discrete number and unit of measurement
☐	☒	An indication of whether measurements were taken from distinct samples or whether the same sample was measured repeatedly
☐	☒	The statistical test(s) used AND whether they are one- or two-sided *Only common tests should be described solely by name; describe more complex techniques in the Methods section.*
☒	☐	A description of all covariates tested
☐	☒	A description of any assumptions or corrections, such as tests of normality and adjustment for multiple comparisons
☒	☐	A full description of the statistics including central tendency (e.g. means) or other basic estimates (e.g. regression coefficient) AND variation (e.g. standard deviation) or associated estimates of uncertainty (e.g. confidence intervals)
☐	☒	For null hypothesis testing, the test statistic (e.g. *F*, *t*, *r*) with confidence intervals, effect sizes, degrees of freedom and *P* value noted *Give P values as exact values whenever suitable.*
☒	☐	For Bayesian analysis, information on the choice of priors and Markov chain Monte Carlo settings
☒	☐	For hierarchical and complex designs, identification of the appropriate level for tests and full reporting of outcomes
☒	☐	Estimates of effect sizes (e.g. Cohen's *d*, Pearson's *r*), indicating how they were calculated
☐	☒	Clearly defined error bars *State explicitly what error bars represent (e.g. SD, SE, CI)*

Our web collection on statistics for biologists may be useful.

Software and code

Policy information about availability of computer code

Data collection

qPCR data were acquired on the CFX Connect Real-Time PCR Detection System(Bio-Rad). Flow cytometry were acquired on a MoFlo Astrios EQS (Beckman Coulter). Hitachi HT-7800 transmission electron microscopy was used to collect data from transmission electron microscopy. Immunoblot images were scanned by azure biosystems c280(Azure). Immunofluorescent images were taken by a Leica SP8 confocal microscope. ZEISS Axio imager.Z2 were used to collect bright field. Leica Aperio Versa 200 were used to collect the immunohistochemical image of human tissues. Richard-wolf was used to take mice intestinal endoscopic images. RNA sequencing were carried out on an BGISEQ-500 sequencer(Beijing Genomics Institute) and HiSeq X-ten sequencer(Illumina). ChIP sequencing were carried out on the HiSeq X-ten sequencer(Illumina).

Data analysis

Image Zen 2.3 blue, black editions, ZEISS Imager. Z2, Las X 2.0.1 and photoshop CS5 were used to analyze bright field or immunofluorescence or immunohistochemical images. Azurespot was used to evaluate the expression of immunoblot images. Flow cytometric analyses were performed with the FlowJo analysis software; Statistical analyses were performed with the GraphPad Prism 6.0 software, SPSS 19.0 and Excel 2017.

Transcriptome RNA-seq: clean reads were aligned to the mouse genome (mm10) by HISAT2. Then gene expression level for each sample was calculated with RSEM. Based on the gene expression level, the differentially expression genes (DEGs) were detected by DEGseq and PossionDis algorithms. Gene set enrichment analysis were performed with gsea 3.0.

RNA-seq for repeats: the 150bp paired-end raw reads were qualified and cleaned by fastp with default setting. Clean reads were mapped onto the mouse genome (GRCm38/mm10) using hisat2. The annotation file of mouse ERVs was generated by RepeatMasker v4.0.7 comparing with Repbase consensus sequences (Edition-20181026). The overlap reads for ERVs were summarized by featureCounts and then quantified by EdgeR.

ChIP-seq: after quality assessment by fastp, clean reads were aligned to the mouse genome (GRCm38/mm10) using Bowtie2 (version 2.2.8). Enriched peaks of H3K9me3 were identified by HOMER v4.10.1 with histone style (http://homer.ucsd.edu/homer). Aligned bam file was converted into the Bigwig file and processed to plot the H3K9me3 density on the interesting ERVs by using deepTools2.0.The original sequencing data is uploaded and available online (Gene Expression Omnibus: GSE129174).

For manuscripts utilizing custom algorithms or software that are central to the research but not yet described in published literature, software must be made available to editors/reviewers upon request. We strongly encourage code deposition in a community repository (e.g. GitHub). See the Nature Research guidelines for submitting code & software for further information.

Data

Policy information about availability of data

All manuscripts must include a data availability statement. This statement should provide the following information, where applicable:

- Accession codes, unique identifiers, or web links for publicly available datasets
- A list of figures that have associated raw data
- A description of any restrictions on data availability

The datasets generated during the current study are available in the GEO dataset with the accession code GSE129174 (https://www.ncbi.nlm.nih.gov/geo/query/acc.cgi?acc=GSE129174). All other data generated in this paper are attached in supplementary materials and source data, source data includes Fig. 1 to Fig. 4 and Extended Data Fig. 1 to Extended Data Fig. 9.

Field-specific reporting

Please select the best fit for your research. If you are not sure, read the appropriate sections before making your selection.

☒ Life sciences ☐ Behavioural & social sciences ☐ Ecological, evolutionary & environmental sciences

For a reference copy of the document with all sections, see nature.com/authors/policies/ReportingSummary-flat.pdf

Life sciences study design

All studies must disclose on these points even when the disclosure is negative.

Sample size	No sample-size calculations were performed. Sample size was determined to be adequate based on the magnitude and consistency of measurable differences between groups.
Data exclusions	On principle, data were only excluded for failed experiments, reasons for which included suboptimal activation, misoperation and microbial contamination. No other strict data were excluded from the study.
Replication	If not stated specifically, experiments were reproduced at least three times. And all attempts at replication were successful.
Randomization	Mice were randomly assigned to control or experimental group.
Blinding	Investigators were not blinded to mouse genotypes during experiments, and blinding was not possible as the authors who performed the experiment also analyzed the data.

Reporting for specific materials, systems and methods

Materials & experimental systems

n/a	Involved in the study
☒	☐ Unique biological materials
☐	☒ Antibodies
☐	☒ Eukaryotic cell lines
☒	☐ Palaeontology
☐	☒ Animals and other organisms
☒	☐ Human research participants

Methods

n/a	Involved in the study
☐	☒ ChIP-seq
☐	☒ Flow cytometry
☒	☐ MRI-based neuroimaging

Antibodies

Antibodies used

Western blotting
anti-Actin(SCBT,sc-81178,ACTBD11B7,lot#L0117,1:4000),anti-GAPDH(SCBT,sc-32233,lot#K0315,1:4000),anti-SETDB1(Proteintech,11231-1-AP,6c5,lot#00070910,1:4000),anti-ZBP1(AdipoGen,AG-20B-0010,Zippy-1,1:4000),anti-MLKL(Proteintech,66675-1-lg,3D4C6,lot#10012588,1:3000),anti-MLKL(phosphorS358)(ABCAM,ab187091,epr9514,lot#GR212667-41,1:2000),anti-MLKL(phosphoS345)（ABCAM ,ab196436, EPR9514,lot#GR3204546-13,1:1000） ,anti-RIP3（ProSci， 2283,lot#8337-1701,1:3000） ,anti-flag(Sigma,f3165,M2,1:4000), Goat anti-Mouse IgG (H+L) Secondary Antibody, HRP (INVITROGEN, 31430, AB_228307,1:10000), Goat anti-Rabbit IgG (H+L) Secondary Antibody, HRP (INVITROGEN,31460, AB_228341,1:10000)
Staining
anti-SETDB1 (Invitrogen, MA5-15722, 5H6A12,lot#RK2296211A, 1:500) ,anti-Lysozyme (Abcam, ab108508, EPR2994(2),lot#GR230-6,1:1000),anti-Mucin2 （SCBT ,sc-15334, H-300,lot#K0315,1:200） , anti-Ki67 （BD Pharmingen, 550609, B56,lot#6195670, 1:1000） , anti-F4/80 (eBioscience,12-4801-80,BM8,lot#E04272-1633, 1:500),anti-CD45(Abcam,ab10558,lot#GR295396,1:500） ,anti-CD45R (B220) (eBioscience,11-0452-85,RA3-6B2,lot#42345301:50),anti-γH2AX （CST ,2577,lot#12, 1:500） ,anti dsRNA J2 （SCICONS,10010200,J2-1717,1:500 ） ,anti-CD3(Abcam,ab5690,lot#GR292058-1,1:500)anti-Ly-6G(Gr-1)(BD Pharmingen,551459,1A8,lot#6294690, 1:500 ） , Cy™3 AffiniPure Donkey Anti-mouse IgG (H+L) （Jackson,715-175-150,1:400 ） ,Cy™3 AffiniPure Donkey Anti-Rabbit IgG (H+L) （Jackson,711-165-152,1:400） , Cy™2 AffiniPure Donkey Anti-Rabbit IgG (H+L) （Jackson,711-225-152,1:400 ） ,Cy™2 AffiniPure Donkey Anti-mouse IgG (H+L) （Jackson ,715-225-150,1:400 ）
Dot Blot
anti-dsRNA J2(SCICONS,10010200,J2-1717, 1μg)
CLIP
anti-ZBP1(AdipoGen, AG-20B-0010, Zippy-1, 1:4000)
IP
anti-ZBP1 (AdipoGen, AG-20B-0010, Zippy-1, 2μg)
CHIP
anti-H3K9me3 (Abcam, ab176916, 30-F1,lot#GR246504-5, 2μg)
FACS
anti-CD24 (eBioscience,12-0241-81, epr16601,1:200)

Validation

All antibodies except p-RIP3(Mus, Home made) are commercially available and have been verified by the manufacturers according to the immunoblots and/or images on their websites.
anti-Actin:https://www.scbt.com/p/beta-actin-antibody-actbd11b7?requestFrom=search
anti-GAPDH: https://www.scbt.com/p/gapdh-antibody-6c5?requestFrom=search
anti-SETDB1: https://www.ptgcn.com/Products/SETDB1-Antibody-11231-1-AP.htm
anti-SETDB1:https://www.thermofisher.com/cn/zh/antibody/product/SETDB1-Antibody-clone-5H6A12-Monoclonal/MA5-15722
anti-ZBP1: https://adipogen.com/ag-20b-0010-anti-zbp1-mab-zippy-1.html
anti-MLKL: https://www.ptgcn.com/products/MLKL-Antibody-66675-1-Ig.htm
anti-MLKL(phosphorS358):https://www.abcam.cn/mlkl-phospho-s358-antibody-epr9514-ab187091.html
anti-MLKL(phosphoS345):https://www.abcam.cn/mlkl-phospho-s345-antibody-epr95152-ab196436.html
anti-RIP3: https://www.prosci-inc.com/rip3-antibody-2283.html,
anti-flag:https://www.sigmaaldrich.com/catalog/product/sigma/f3165?lang=zh&region=CN
Goat anti-Mouse IgG (H+L) Secondary Antibody, HRP: https://www.thermofisher.com/cn/zh/antibody/product/Goat-anti-Mouse-IgG-H-L-Secondary-Antibody-Polyclonal/31430
Goat anti-Rabbit IgG (H+L) Secondary Antibody, HRP: https://www.thermofisher.com/antibody/product/Goat-anti-Rabbit-IgG-H-L-Secondary-Antibody-Polyclonal/31460
anti-Lysozyme: https://www.abcam.cn/lysozyme-antibody-epr29942-ab108508.html
anti-Mucin2: https://www.scbt.com/p/mucin-2-antibody-h-300?requestFrom=search
anti-Ki67:https://www.bdbiosciences.com/cn/applications/research/intracellular-flow/intracellular-antibodies-and-isotype-controls/anti-rat-antibodies/purified-mouse-anti-ki-67-b56/p/550609
anti-F4/80:https://www.thermofisher.com/cn/zh/antibody/product/F4-80-Antibody-clone-BM8-Monoclonal/12-4801-80
anti-CD45: https://www.abcam.com/cd45-antibody-ab10558.html
anti-CD45R:https://www.thermofisher.com/cn/zh/antibody/product/CD45R-B220-Antibody-clone-RA3-6B2-Monoclonal/11-0452-85
anti-γH2AX:https://www.cst-c.com.cn/products/primary-antibodies/phospho-histone-h2a-x-ser139-antibody/2577
anti dsRNA J2: https://scicons.eu/en/antibodies/j2/
anti-CD3: https://www.abcam.com/cd3-antibody-ab5690.html
anti-Ly-6G(Gr-1):https://www.bdbiosciences.com/cn/reagents/research/antibodies-buffers/immunology-reagents/anti-mouse-antibodies/cell-surface-antigens/purified-rat-anti-mouse-ly-6g-1a8/p/551459 Cy™3 AffiniPure Donkey Anti-mouse IgG (H+L): https://www.jacksonimmuno.com/catalog/products/715-175-150
Cy™3 AffiniPure Donkey Anti-Rabbit IgG (H+L): https://www.jacksonimmuno.com/catalog/products/711-165-152
Cy™2 AffiniPure Donkey Anti-Rabbit IgG (H+L): https://www.jacksonimmuno.com/catalog/products/711-225-152
Cy™2 AffiniPure Donkey Anti-mouse IgG (H+L): https://www.jacksonimmuno.com/catalog/products/715-225-150
anti-CD24:https://www.thermofisher.com/cn/zh/antibody/product/CD24-Antibody-clone-30-F1-Monoclonal/12-0241-81
anti-H3K9me3:https://www.abcam.cn/histone-h3-tri-methyl-k9-antibody-epr16601-chip-grade-ab176916.html
All antibodies are commercial and were validated by manufacturers for indicated species and applications except phospho-RIPK3 was produced by Jiahuai Han lab and licensed to ABCAM (AB205421) as validated in supplementary figure 4.

Eukaryotic cell lines

Policy information about cell lines

Cell line source(s)	293T and L929 were purchased from ATCC.
Authentication	Cell line from ATCC has been authenticated by ATCC. The primary lines are cultured for limited number of passages.
Mycoplasma contamination	Cell lines tested negative for Mycoplasma contamination.
Commonly misidentified lines (See ICLAC register)	No commonly misidentified cell lines were used.

Animals and other organisms

Policy information about studies involving animals; ARRIVE guidelines recommended for reporting animal research

Laboratory animals	All mice were in C57BL/6 background and housed in a conventional environment under a 12-hour light: dark cycle at the Xiamen University Laboratory Animal Center. VilCreERT2; Setdb1fl/fl mice were crossed with Casp8fl/fl, Mlkl-/-, Rip3-/- or Zbp1-/- mice to generate inducible double knock out mice, respectively. VilCreERT2 or Olfm4-CreERT2 mice were received one dose of tamoxifen 400 mg/kg by gavage with 8 weeks old mice. Lgr5-EGFP-IRES-CreERT2; Setdb1fl/fl mice were received one dose of tamoxifen 200mg/kg by gavage for three consecutive days with 8 weeks mice. Sample sizes for mouse experiments were empirically determined, and mice were randomly assigned to control or experimental group. For all experiments, littermates were used as control indicated in each figure. No blinding was necessary for the mouse experiments present here. Gender preference was not existed in bowel inflammatory mice model here.For more reference information please see Supplementary Table 1.
Wild animals	The study did not involve wild animals.
Field-collected samples	The study did not involve samples collected from the field.

ChIP-seq

Data deposition

☒ Confirm that both raw and final processed data have been deposited in a public database such as GEO.

☐ Confirm that you have deposited or provided access to graph files (e.g. BED files) for the called peaks.

Data access links *May remain private before publication.*	https://www.ncbi.nlm.nih.gov/geo/query/acc.cgi?acc=GSE129174
Files in database submission	input_1.fq.gz input_2.fq.gz ChIP_H3K9me3_1.fq.gz ChIP_H3K9me3_2.fq.gz H3K9me3peaks.txt.gz WT.fq.gz VEMD2.fq.gz VEMD3.fq.gz VEMD4.fq.gz VEMD6.fq.gz VEMD8.fq.gz ISC_WT_1.fq.gz ISC_WT_2.fq.gz ISC_MUT_1.fq.gz ISC_MUT_2.fq.gz RNA_expression_days.txt.gz RNA_expression_ERVs.txt.gz
Genome browser session (e.g. UCSC)	http://genome.ucsc.edu/cgi-bin/hgGateway Integrative Genomics Viewer (IGV, version 2.4.5).

Methodology

Replicates	ChIP sequencing analysis of lgr5-postive cells were performed once.
Sequencing depth	Library concentrations were mixed equally for sequencing at Hiseq-Xten to generate 150 bp reads from paired-end.
Antibodies	anti-H3K9me3 Abcam ab176916

Peak calling parameters	Clean reads were aligned to the mouse genome (GRCm38/mm10) using Bowtie2 (version 2.2.8). Enriched peaks of H3K9me3 were identified by HOMER v4.10.1 with histone style (http://homer.ucsd.edu/homer).
Data quality	Peaks were called using an input control. Peaks were called at an FDR of 0.1% and required 4-fold enrichment over the input control.
Software	bowtie2; homer; fastp0.19.0; deepTools2.0

Flow Cytometry

Plots

Confirm that:

☒ The axis labels state the marker and fluorochrome used (e.g. CD4-FITC).

☒ The axis scales are clearly visible. Include numbers along axes only for bottom left plot of group (a 'group' is an analysis of identical markers).

☒ All plots are contour plots with outliers or pseudocolor plots.

☐ A numerical value for number of cells or percentage (with statistics) is provided.

Methodology

Sample preparation	Crypts from Lgr5-EGFP-IRES-CreERT2;Setdb1fl/fl mice were used and digested into single cells with 0.25% Trypsin above ice and pipetted for 2-3min till most crypts dissociated, then terminated with FBS containing medium and filled through 50um filter. After centrifugation 1200 rpm/5min, stained with CD24-PE antibody for 20min, then resuspended with PBS for FACS.
Instrument	MoFlo Astrios EQS, Beckman Coulter
Software	FlowJo
Cell population abundance	For RNA-seq for repeats, at least 1,000,000 GFP high CD24 low ISCs were collected for each genotype, for ISCs specific ChIP, at least 3,000,000 GFP high CD24 low cells were collected.
Gating strategy	Positive and negative gates were set using fluorescence minus one (FMO) background intensity controls. Detailed gating strategy is provided under supplementary figure 6.

☒ Tick this box to confirm that a figure exemplifying the gating strategy is provided in the Supplementary Information.